Nanobody GPS by PCS: an efficient new NMR analysis method for G protein coupled receptors and other large proteins

Feng-Jie Wu[a], Pascal S. Rieder[b], Layara Akemi Abiko[a], Philip Rößler[c], Alvar D. Gossert[c*], Daniel Häussinger[b*], Stephan Grzesiek[a*]

[a] Biozentrum, University of Basel, CH-4056 Basel, Switzerland
[b] Department of Chemistry, University of Basel, CH-4056 Basel, Switzerland
[c] Department of Biology, ETH Zürich, 8093 Zürich, Switzerland

*Address correspondence to:
Stephan Grzesiek
Biozentrum, University of Basel, CH-4056 Basel, Switzerland
Phone: ++41 61 207 2100
FAX: ++41 61 207 2109
Email: Stephan.Grzesiek@unibas.ch

Daniel Häussinger
Department of Chemistry, University of Basel, CH-4056 Basel, Switzerland
Phone: ++41 61 207 11 59
Email: daniel.haeussinger@unibas.ch

Alvar Gossert
Department of Biology, ETH Zürich, 8093 Zürich, Switzerland
Phone: +41 44 663 34 55
Email: alvar.gossert@mol.biol.ethz.ch

Keywords: pseudocontact shift, high-resolution NMR, antibody, DOTA, paramagnetism, lanthanide, electronic forces

Abstract

NMR chemical shift changes can report on the functional dynamics of biomacromolecules in solution with sizes >1 MDa. However, their interpretation requires chemical shift assignments to individual nuclei, which for large molecules often can only be obtained by tedious point mutations that may interfere with function.

We present here an efficient pseudocontact shift NMR method to assign biomacromolecules using bound antibodies tagged with lanthanoid DOTA chelators. The stability of the antibody allows positioning the DOTA tag at many surface sites, providing triangulation of the macromolecule nuclei at distances >60 Å. The method provides complete assignments of valine and tyrosine ^{1}H-^{15}N resonances of the β_1-adrenergic receptor in various functional forms. The detected chemical shift changes reveal strong forces exerted onto the backbone of transmembrane helix 3 during signal transmission, which are absorbed by its electronic structure. The assignment method is applicable to any soluble biomacromolecule for which suitable complementary binders exist.

Introduction

The observation of resonances of magnetically active atomic nuclei can provide invaluable information on the functional motions of biomacromolecules, which often remain undetected in static crystallographic or cryo-EM structures. For the interpretation of the observed resonances, the assignment of their frequencies to the corresponding nuclei is a prerequisite. Nuclear magnetic resonance (NMR) techniques developed over the last decades can achieve the complete backbone assignments for proteins up to about 80 kDa based on scalar couplings between ^{1}H, ^{13}C and ^{15}N nuclear spins[1]. However, this approach is not practical for larger proteins due to fast transverse relaxation rates, which render the scalar magnetization transfer inefficient. In addition, resonance overlap in large proteins makes it particularly difficult to interpret multiple states with similar chemical shifts. Albeit specific isotope labeling can effectively reduce spectral complexity, the sparsity of unconnected spins further aggravates the problem of resonance assignments. Hence, more effective assignment methods are urgently needed for the NMR analysis of large proteins.

In principle, pseudocontact shifts (PCSs) induced by unpaired electrons onto magnetic nuclei may provide such an assignment tool, since they can be easily observed over large distances (60 Å and beyond) and depend in a well-defined manner on the relative geometry of the electron and the nucleus. Initially, metalloproteins have been explored for this purpose, since their natively bound metal can often be substituted with a paramagnetic metal harboring unpaired electrons[2]. Indeed, ^{1}H-^{15}N backbone[3] and ^{1}H-^{13}C methyl side chain[4] resonance assignments of selectively labeled amino acids have been achieved in a 30-kDa complex of a metalloprotein based on PCS information. In a considerably larger, 300-kDa metalloprotein system, PCS helped the assignment of methyl resonances by resolving ambiguities encountered from an NOE approach[5]. For non-metal-binding proteins, the paramagnets need to be introduced by tagging the protein with suitable labels. This may be achieved by genetically encoding metal-binding peptide sequences into loops or terminal regions[6,7] or by chemically coupling synthetic paramagnetic tags to the protein surface at introduced cysteines or other residues[8,9]. A high rigidity of the tag itself[10] and minimal motion of the tag relative to the protein[11] are prerequisites for strong PCS. Furthermore, if the PCSs should be useful for ab initio assignments more than one paramagnetic position is needed to resolve ambiguities in the three-dimensional geometry dependence of the one-dimensional PCS observation. In practice, multiple tagging sites need to be screened before a single reasonably rigid tagging site can be found. This may require deleting native cysteine residues and inserting new ones or using non-natural amino acids, which is a laborious and pitfall-prone process. This problem is aggravated by the fact that sensitive proteins

may be affected in their function or even denatured by the introduction of the label. Thus, paramagnetic labeling at multiple sites constitutes a formidable practical problem.

G protein-coupled receptors (GPCR) present an important, but challenging target for the dynamical analysis by solution NMR. They are transmembrane proteins which regulate many vital functions of the human body by recognizing extracellular ligands and transmitting this stimulus to intracellular signaling cascades[12]. Their function is achieved via highly dynamic equilibria between multiple active and inactive conformations, which are modulated by the ligands[13–24]. Atomic details of these dynamical equilibria and their driving forces are still largely unknown.

We have recently analyzed these functional conformational equilibria by NMR in a variant of the turkey β_1-adrenergic receptor (YY-β_1AR), which was stabilized by point mutations and expressed in insect cells with ^{15}N-valine isotope labeling on a non-deuterated background[14,15,25]. The total mass of the detergent-solubilized receptor exceeds 100 kDa[14]. Point mutations and proximity arguments provided 17 certain and 4 tentative assignments of the 28 observed ^{1}H-^{15}N correlations in two-dimensional TROSY spectra of YY-β_1AR in an inactive conformation in complex with antagonists. Agonist-bound complexes showed a dynamical equilibrium between a preactive and an active conformation[14]. The active conformation largely corresponds to the conformation in ternary complexes with G protein or G protein-mimicking nanobodies (Nbs) where TM5 and TM6 have moved outward to accommodate the G protein/Nb[26]. However, only 8 confirmed or tentative assignments could be obtained for the fully active conformation, since many of the introduced point mutations abolished the transition to the active conformation. The missing assignments precluded a full analysis of the dynamical equilibrium between the preactive and the active conformation. Attempts to obtain assignments by paramagnetic tags directly coupled to the receptor via introduced cysteines failed due to receptor instability and interference with its intrinsic cysteines and disulfide bridges.

Here we resolve this problem of the NMR assignment of the β_1AR by coupling the thulium-loaded, rigid DOTA-M7PyridineThiazole variant (Tm-DOTA-M7PT)[10,27] via nucleophilic aromatic substitution, S_NAr, of a cysteine thiolate to nanobodies that specifically bind β_1AR in various functional states. The robustness of the nanobodies allows easy tagging at multiple positions, thereby triangulating the atoms of the receptor and resolving the assignment ambiguities. For this reason, we term the method GPS-PCS (Global Positioning System for PCS). Using the GPS-PCS approach in combination with the known three-dimensional structures of the receptor•nanobody complexes, complete ^{1}H-^{15}N-valine assignments were obtained for several functional receptor states, which revealed hitherto undetected forces onto

the backbone of TM3 during activation. Once the PCS tensors are determined, the assignments are easily extended to other resonances of specifically labeled amino acids, such as ^{15}N-tyrosine. The method should be generally applicable to all biomacromolecules for which suitable antibody binders exist.

Results and Discussion

Efficient selection of DOTA labeling sites on nanobodies

To obtain large PCS values containing maximally independent information, the Tm-DOTA tag should be attached as rigidly as possible via its aromatic linker to cysteine point mutations at several distinct positions of the nanobody. Ideal attachment sites must be accessible for labeling but will also restrict the motions of the formed pyridine thiazole-cysteine linker. To develop a rational and efficient approach for the selection of such optimal attachment sites, we created a rotamer library of the Tm-DOTA-M7PT-cysteine residue (Figure 1A) with side chain angles at staggered rotamer positions, i.e. $\chi_{1/2} = \pm 60^\circ$, 180° and $\chi_3 = \pm 90^\circ$. Nanobody amino acid positions were then screened by placing the resulting 18 DOTA-cysteine rotamers (Figure 1B) with their N, C^α and C' atoms at the corresponding nanobody backbone positions. Steric clashes at every amino acid position were quantified by a simple sum of van der Waals radii penetrations (Σ_{vdwp}) for every rotamer (Figure 1C). Typically, a $\Sigma_{vdwp} < \sim 100$ Å of at least one of the 18 rotamers corresponded to an amino acid position on the surface of the nanobody. The expected rigidity of the DOTA-cysteine tag was estimated by counting the number of rotamers with a Σ_{vdwp} below a certain threshold (60 Å proved practical). A low number of such rotamers is expected to yield an attached DOTA tag with high rigidity and correspondingly large PCS effect.

Since we were lacking almost all assignments of YY-β_1AR in its active conformation, we initially screened amino acids within Nb80, which binds to the agonist-bound receptor in a similar manner as the G protein[28], using the crystal structure of β_1AR in complex with the agonist isoprenaline and Nb80 (PDB 6h7j)[29]. From all Nb80 residues with a $\Sigma_{vdwp} < 60$ Å for at least one rotamer, we selected 7 distributed at geometrically distinct positions close to the receptor (Figure 1C,D, green). All of these residues could be mutated to cysteines and easily tagged by Tm-DOTA-M7PT. The observed ^{1}H PCS size (rms value) of all receptor valine residues for the isoprenaline·YY-β_1AR complexes with these Nb80 mutants confirmed that the number of allowed rotamers below the 60-Å Σ_{vdwp} threshold provided a crude first approximation of the expected PCS size (Figure 1C). Namely, residues S25 and S70 with ≥ 8 allowed rotamers had a very small PCS rms, whereas Q39, T57, Y107, and D108 with ≦ 4 allowed rotamers had a large PCS rms. An exception is N76 with only 1 allowed rotamer but a

very small PCS rms. In contrast to the other residues, N76 is located in a turn, which may cause additional backbone flexibility as well as large inaccuracies in steric clashes predicted from the cryogenic crystal structure due to the flexibility of adjacent side chains under solution conditions. Nevertheless, with a success rate of 4/5 this simple computational procedure provides a good guideline for the design of suitable nanobody mutants.

GPS-PCS based assignment strategy

To develop a robust assignment strategy, we concentrated first on three of the four Tm-DOTA-tagged nanobody mutants with the largest observed PCS rms, namely Nb80-Q39C, Nb80-T57C, Nb80-D108C, which are distributed at distinct positions within the nanobody (Figure 2A). ^{1}H-^{15}N TROSY spectra of these mutants in complex with ^{15}N valine-labeled isoprenaline•YY-β_1AR are shown in Figure 2B-D in comparison with the diamagnetic ^{15}N valine-labeled isoprenaline•YY-β_1AR•Nb80-wt (wild-type) complex. The peak centers of the ^{1}H-^{15}N resonances of individual amino acids are located on straight lines with slope 1 for the paramagnetic and diamagnetic complexes (Figure 2E) as expected from the relative proximity of their amide ^{1}H and ^{15}N nuclei in comparison to the large (20–65 Å) amide-paramagnetic center distance. The sparseness and good resolution of the ^{1}H-^{15}N correlations allowed unambiguous assignment of almost all paramagnetic and diamagnetic cross peaks to a single amino acid resonance.

To use the observed PCSs for assignment, an accurate definition of the PCS tensors of the Tm-DOTA-tagged nanobody mutants is needed. Each tensor is defined by five intrinsic parameters as well as the three cartesian coordinates of the paramagnetic center. Due to the large distances of the paramagnetic centers to the receptor, their positions are well approximated as an average of Tm coordinates from the different DOTA-cysteine rotamers weighted by their van der Waals penetrations (see Methods). Initial assignment information for the ^{1}H-^{15}N resonances of V62$^{1.53}$, V122$^{3.33}$, V129$^{3.40}$, V172$^{4.56}$, V202^{ECL2}, and V314$^{6.59}$ [superscripts indicate Ballesteros-Weinstein numbering[30]] of the isoprenaline•YY-β_1AR•Nb80 complex was available from six point mutations[14,15]. These were used to obtain starting values for the ^{1}H PCS tensors of the three Tm-DOTA-M7PT-tagged Nb80 complexes by fitting the observed PCS values with coordinates derived from three-dimensional structures of the complex and the rotamer-averaged Tm paramagnetic center positions. Clearly, these tensors are not yet well defined as the five intrinsic tensor parameters are derived from only six PCSs.

For a further refinement of the tensors, we sought assignment of the 10 most well-resolved, unassigned resonances in the ^{1}H-^{15}N TROSY spectra (marked in blue in Figure 2K) by the following procedure (Figure 2F). We first calculated theoretical PCS values for all 28 valine ^{1}H

resonances in the receptor using the initial tensor parameters and the coordinates of the receptor. These were then compared by a chi-square cost function relative to all observed 28 PCS values for all tensors, yielding a 28x28 cost matrix for possible assignments. For each of the 10 well-resolved resonances, an assignment candidate was defined as the residue, which yielded the smallest chi-square. Each of these tentative assignments was then tested to obtain a tentative refined PCS tensor and a new 28x28 cost matrix. Using the latter cost matrix, a tentative total assignment of all resonances with minimal total chi-square was obtained by solving the respective combinatorial minimization problem (Figure 2G) using an efficient linear programing approach[31]. The definitive next assignment was then taken as the tentative assignment with the smallest total chi-square. This procedure was repeated recursively for the remaining well-resolved resonances.

With the assignments augmented to 16, the final assignments of the remaining 12 resonances in the crowded region of the spectrum (marked in red in Figure 2K) were derived using again the smallest total chi-square solution of the cost matrix obtained by the linear programing algorithm. A comparison with previous assignments of the antagonist-bound forms of the receptor revealed one single inconsistency, namely an interchange of V102$^{2.64}$ and V326$^{7.36}$, which are very close in the structure and have nearly identical PCSs. After fixing these two assignments to their expected values, the linear programing solution for the smallest total least square of the cost matrix provided all other assignments automatically (Figure 2H). The agreement between experimental and predicted ^{1}H PCS values is excellent (rmsd < 22 ppb, Pearson r > 0.997) for all three Nb80 DOTA-tagged mutants, and a visualization of the respective tensors reveals highly distinct spatial distributions of their induced pseudocontact magnetic fields (Figure 2J).

For a quality control of this simultaneous assignment and PCS tensor refinement, it is instructive to analyze the development of the tensor parameters during this procedure (Figure 2I). Whereas the tensor parameters (amplitude and direction cosines) derived from the six initial valine assignments deviate very strongly (e.g. more than 10-fold in amplitude for Nb80-Q39C) from the tensors of the final assignment of all 28 valines, the parameters quickly converge towards their final values after the addition of 3–5 more assignments. It should be noted that the automated assignment procedure via the smallest total chi-square solution of the cost matrix provided correct results for >80% of the unassigned resonances already with only the first 7–8 assignments defining the PCS tensors.

Complete assignment of backbone valines in multiple states of YY-β_1AR

Using the same GPS-PCS approach as for the active-state YY-β_1AR we also sought to complete the assignments of the ^{1}H-^{15}N valine resonances of the inactive receptor. Definite or tentative assignments had been achieved previously for 21 of the 28 valines by direct point mutations and proximity effects[14,15]. The nanobody Nb60 binds to the inactive form of the receptor[32]. Compared to the binary complex of YY-β_1AR with the antagonist carvedilol, the ternary carvedilol•YY-β_1AR•Nb60 exhibits only minor ^{1}H-^{15}N chemical shift changes, appearing for valines located close to the receptor nanobody binding site (Figure S1). Similarly only very small ^{1}H-^{15}N chemical shift changes are observed for the ^{1}H-^{15}N tyrosine resonances (Figure 2A, see below) of the carvedilol•YY-β_1AR complex upon Nb60 binding. Thus, there are only very small conformational changes induced by Nb60, which is expected since this nanobody was selected as a binder to the inactive conformations of the highly homologous β_2AR receptor[32].

In silico screening of Nb60 (PDB 5jqh, with β_2AR replaced by β_1AR PDB 4amj) for good DOTA labeling positions revealed similar candidate mutation sites, of which Nb60-Q39C, Nb60-N57C, Nb60-D107C (equivalent to residue 108 in Nb80) yielded strong induced PCS in the complexes of carvedilol•YY-β_1AR with the DOTA-tagged Nb60 variants. Using the identical procedure as for the active YY-β_1AR, but based on a much larger set of pre-assigned resonances, complete assignments besides an ambiguity of the close-by pairs V51$^{1.42}$/V52$^{1.43}$ and V309$^{6.54}$/V312$^{6.57}$ could be obtained for the inactive carvedilol•YY-β_1AR complex. During this process, previous tentative assignments by proximity effects for V56$^{1.47}$, V62$^{1.53}$, V89$^{2.52}$, V134$^{3.45}$ were also corrected.

Due to relatively small chemical shift differences, the assignment of the carvedilol•YY-β_1AR ^{1}H-^{15}N valine resonances is easily transferred to spectra of the YY-β_1AR apo form as well as further binary complexes, such as the preactive isoprenaline•YY-β_1AR (Figure 3A, B). In contrast, the binding of Nb80 to the isoprenaline•YY-β_1AR complex and the subsequent formation of the fully active conformation induces significantly larger chemical shift perturbations [CSP = $\left(\Delta\delta_N{}^2/25 + \Delta\delta_{HN}{}^2\right)^{1/2}$] throughout the receptor, which had previously impeded the assignment by chemical shift proximity (Figure 3C, D). Valines are widely distributed in β_1AR, including the extracellular ligand binding region, the mid region, and the intracellular G protein coupling region (Figure 3E). The availability of almost complete ^{1}H-^{15}N valine resonance assignments allows now to track relevant structural backbone perturbations throughout YY-β_1AR in multiple states (Figure 3A-C), including the highly dynamic apo and

agonist-bound intermediate states, which are inaccessible to high-resolution structure determination but are key to understanding function.

Relative to the apo state, significant (>0.1 ppm) CSPs are detected in the orthosteric ligand-bound forms for many valines surrounding the ligand pocket (V122$^{3.33}$, V125$^{3.36}$, V172$^{4.56}$) and extending into the extracellular ends of TM5-7 (V202^{ECL2}, V314$^{6.59}$, V326$^{7.36}$), indicating that signal initiation by the orthosteric ligand affects the whole extracellular region adjacent to the ligand pocket. Remarkably, the apo or isoprenaline-bound preactive receptor forms (Figure 3B) have broader line widths than the carvedilol-bound inactive (Figure 3A) and the ternary active complexes (Figure 3C), consistent with the notion that the former undergo exchange between several conformations on the micro- to millisecond time scale, whereas such exchange is largely impeded for the latter[14]. In the presence of the full agonist isoprenaline, we previously reported that backbone valines in the extracellular region undergo slow exchange between the preactive (~80% population) and the active conformation (~20% population)[14]. With the current complete assignment in the active state, this phenomenon is observed for many further valines in the extracellular and the mid regions (Figure 3D, E).

Activation by Nb80 induces strong forces on the receptor backbone at specific locations

Whereas the binary orthosteric ligand complexes show CSPs relative to the apo form of at most 0.4 ppm, considerably larger CSPs of up to 1.8 ppm are observed for certain residues when Nb80 forms a ternary complex with the isoprenaline-bound YY-β_1AR (Figure 3D). Relative to the isoprenaline•YY-β_1AR complex, the CSPs are particularly strong (0.5< CSP <1.8ppm) for valines in TM2, TM3, TM5 and TM6 (Figure 4A, B). These perturbations of the ^{1}H-^{15}N chemical shifts report on changes in the electron density surrounding these nuclei, which are caused by variations in hydrogen bonding and backbone conformation[33,34]. Thus, the strong ^{1}H-^{15}N CSPs give evidence of considerable forces exerted onto the receptor backbone at specific locations by Nb80 binding.

The strong CSPs induced by Nb80 at the intracellular side of TM5 (V226$^{5.57}$, V230$^{5.61}$) and TM6 (V298$^{6.43}$) can be rationalized by the large outward motion of TM5 and TM6 away from the transmembrane 7-helix bundle that accommodates the G protein or Nb80 binding in the fully active conformation[28,35]. Furthermore, the very strong CSP of V314$^{6.59}$ at the extracellular end of TM6 has been explained previously by a pivoting of TM6 around its center as the Nb80 pries the intracellular part of TM6 away from the helix bundle and pushes its extracellular part towards TM5[14]. This inward motion of the extracellular end of TM6 compacts the ligand binding pocket and increases the affinity for agonists. We now see from the very strong CSP of V298$^{6.43}$, preceding F299$^{6.44}$ of the PIF motif, that the mid of TM6 also experiences considerable strain

during this motion. Further smaller, yet sizeable CSPs (Figure 4C, D) accompany the compaction of the binding pocket in its vicinity on TM2 (V89$^{2.52}$, V90$^{2.53}$, V94$^{2.56}$, V95$^{2.57}$, V102$^{2.64}$), TM4 (V165$^{4.49}$, V172$^{4.56}$), and ECL2 (V202^{ECL2}) as well as the overall activating motion in TM1 (V51$^{1.42}$, V52$^{1.43}$, V60$^{1.51}$, V62$^{1.53}$).

TM3 is a crucial stabilizing hub absorbing forces exerted by receptor activation in its electronic structure

Surprisingly, we also observe very large CSPs upon Nb80 binding for all valines (V122$^{3.33}$, V125$^{3.36}$, V129$^{3.40}$ and V134$^{3.45}$) in TM3 (Figure 4A-C). The importance of TM3 as a central stabilizing hub for the inactive and active conformation was previously postulated based on residue-residue contacts[36,37]. However, no large structural changes are observed in the mid and extracellular parts of TM3 of class A receptors upon activation and only its intracellular part undergoes a rotation of e.g. 37° in the β_2AR[36]. The very strong ^{1}H-^{15}N CSPs induced in the TM3 of β_1AR by Nb80 binding show that the forces exerted onto the TM3 backbone by the activating motions extend much beyond its intracellular side and reach V129$^{3.40}$, V125$^{3.36}$, and V122$^{3.33}$ at its mid and extracellular side. Thus, TM3 appears to act as central stabilizing hub, which does not change significantly its backbone positions upon activation, but rather absorbs the occurring forces within its electronic structure as evidenced by the strong ^{1}H-^{15}N CSPs.

Extension of assignments to other specifically labeled residues

With the PCS tensors available for the different DOTA-tagged Nb mutants, it is straightforward to extend the assignments to other nuclei in the various states of the receptor. As an example, we show the assignment of ^{15}N-labeled tyrosines. Tyrosines are essential parts of the canonical microswitch network involved in the activation of class A GPCRs, such as Y140$^{3.51}$ within the conserved DRY motif and Y227$^{5.58}$/Y343$^{7.53}$ within the TM5/TM7 YY-bridge/NPxxY motifs[14,38,39]. In the inactive conformation, the side chain of Y343$^{7.53}$ orients towards the side chain of N339$^{7.49}$ in the NPxxY motif forming a water-mediated H-bond network, while the side chain of Y227$^{5.58}$ points towards the intracellular opening of the TM bundle. In contrast, in the active conformation, the side chains of Y227$^{5.58}$ and Y343$^{7.53}$ face each other and connect via a water molecule, thereby subtending TM6 and stabilizing its swung-out conformation[14].

Assignment of the key tyrosines Y227$^{5.58}$ and Y343$^{7.53}$ by point mutations in the active conformation is impossible since such mutations abolish the formation of the active conformation and binding of G protein or Nb80[14,15]. However, the assignments of all ^{1}H-^{15}N resonances of the ^{15}N-tyrosine-labeled receptor in its active conformation were easily obtained by the PCSs measured in only two complexes with the paramagnetic Tm-DOTA-M7PT-Nb80-

Q39C and -T57C (Figure 5A). A comparison to the PCS values predicted from the previously derived PCS tensors uniquely identified 8 out of 9 tyrosines (Figure 5B). The only remaining unassigned tyrosine resonance of the diamagnetic Nb80-wt complex was very weak, and no corresponding resonances were observed in the paramagnetic Nb80 complexes. This resonance was tentatively assigned to $Y149^{ICL2}$ as the only remaining tyrosine. $Y149^{ICL2}$ is very close to the Nb80 interface, its predicted paramagnetic shifts are very strong, and the resonances are presumably broadened due to conformational exchange. It is interesting to note that the ^{1}H-^{15}N resonances of $Y140^{3.51}$ and $Y227^{5.58}$ overlap in the diamagnetic spectrum, but are well separated in the paramagnetic spectra providing a clear assignment. The assignment of all tyrosines in the inactive carvedilol•YY-β_1AR•Nb60 complex was achieved in an analogous way using the PCS information from only one paramagnetic complex with Tm-DOTA-M7PT-Nb60-Q39C and the proximity of active-state resonances (Figure S2).

The obtained tyrosine assignments were easily transferred to the binary YY-β_1AR complexes with carvedilol and isoprenaline by the close proximity of resonances, providing comprehensive chemical shift information on the inactive, preactive, and active states of the receptor (Figure 5C, D). A comparison between the inactive (carvedilol•YY-β_1AR) and preactive (isoprenaline•YY-β_1AR) complexes reveals a very strong (0.32 ppm) CSP for $Y333^{7.43}$ whereas all other resonances are only moderately (<0.15 ppm) shifted (Figure 5E). $Y333^{7.43}$ resides very close to the orthosteric pocket and apparently strongly senses the difference between the agonist and antagonist chemical structure. Of note, the side chain of the equivalent $M287^{7.43}$ in the chemokine receptor CCR5 has recently been shown to be crucially involved in its activation[40]. Similar to the splitting of some of the ^{1}H-^{15}N valine resonances in the isoprenaline•YY-β_1AR complex corresponding to the preactive and active conformations, also the ^{1}H-^{15}N $Y333^{7.43}$ resonance is split into a major resonance for the preactive and a minor resonance for the active conformation, the latter being very close to the $Y333^{7.43}$ resonance of the ternary isoprenaline•YY-β_1AR•Nb80 complex (Figure 5C, D). Finally, the strongest tyrosine CSPs are observed between the fully active conformation in the isoprenaline•YY-β_1AR•Nb80 complex and the preactive conformation with CSPs > 0.25 ppm not only for $Y140^{3.51}$, $Y227^{5.58}$ and $Y343^{7.53}$ of the DRY and YY-bridge/NPxxY motifs, but also for $Y217^{5.48}$ and $Y231^{5.62}$ (Figure 5F) in agreement with the strong structural perturbation of TM5.

Conclusions

Due to its ~100 kDa overall size, conventional triple-resonance assignment methods fail for the detergent-solubilized, non-deuterated β_1AR produced from insect cells. Although a number of ^{1}H-^{15}N valine resonances could be assigned by tedious point mutations for the inactive and

preactive β_1AR[14,15], the latter approach proved mostly infeasible for the active receptor as many mutations abrogated receptor function and impeded the transition to the active conformation. The instability of β_1AR also prevented assignments via PCS induced by paramagnetic tags directly attached to the receptor via cysteine chemistry. In contrast, tagging the β_1AR-binding nanobodies by the rigid Tm-DOTA-M7PT is straightforward and very robust. Many tagging sites are possible, as nanobodies are evolved to be highly stable. The best tagging positions can even be predicted to a certain extent by a simple analysis of sterically allowed cysteine-M7PT-DOTA side chain rotamers. In this respect, it is interesting to observe that the used tagging sites still allow a certain flexibility of the paramagnetic label, since the tensor amplitudes (A_{zz} and rhombicity, Table S2) vary appreciably between the sites. This is also consistent with the varying number of allowed rotamers according to the rotamer van der Waals clash analysis. An improvement of the predictions of suitable tagging sites and a better understanding of DOTA flexibility seems possible via full-scale molecular dynamics simulations of the nanobody-cysteine-M7PT-DOTA system.

The observed PCSs induced by the thulium-loaded, rigid DOTA-M7PT tag are detectable with high sensitivity and accuracy at metal-nuclear distances even beyond 60 Å, while PRE effects are very moderate. Even larger distances of up to about 100 Å may become detectable using the even more rigid DOTA-M7Nitro tag with dysprosium loading[41]. It is also noted that the inactive conformation of the receptor as monitored by the ^{1}H-^{15}N resonances of valines and tyrosines is very little affected by the binding of the Nb60, whereas the receptor conformation in the Nb80-bound state is highly similar to the G protein-bond state. This can be expected for most antibody binders when they are developed to recognize specific conformations as in the case of Nb60[32] and Nb80[28].

The information content of the PCS values induced by three different Tm-DOTA-M7PT labeling sites was sufficient to automatically assign almost all 28 (besides the interchange of the nearby residues V102$^{2.64}$ and V326$^{7.36}$) ^{1}H-^{15}N valine resonances of the ^{15}N-valine-labeled active isoprenaline·YY-β_1AR·Nb80 complex from only six pre-assigned valine residues and its known three-dimensional structure. The method hinges on the geometric information content of the various PCS values observed for a single nucleus. Independence of the information is achieved here by the variation of the paramagnetic tag positions. Additional information may be obtained by changing the paramagnetic lanthanides within the same DOTA tag leading to a change of the tensor amplitudes and directions. However, the latter may provide less independent information since the tensor parameters are expected to be linearly dependent.

It should be noted that automated assignment from PCS values is much simpler than from NOEs, since the function predicting the PCS value depends on the coordinates of only a single nucleus and not of a pair of nuclei. This gives the related cost function the form of a matrix trace, which can be effectively optimized by a matrix permutation using a linear programming approach. An equivalent solution is obtained by the 'Hungarian method'[3,42] Further simple extensions of this approach are possible for incomplete or ambiguous observations of PCS values. Once the PCS tensor parameters were determined from the ^{15}N-valine resonance, they could easily be transferred to obtain full assignments of selectively ^{15}N-tyrosine labeled constructs, which hitherto was impossible due to the functional importance of key residues like Y227$^{5.58}$ and Y343$^{7.53}$. It is obvious that the transfer of the tensor parameters and the same assignment strategy can be applied to many other selective or even uniform labeling schemes. Hence, GPS-PCS provides efficient assignments for unconnected magnetic nuclei in large systems without resorting to laborious and distorting mutagenesis.

Nanobody binders have been developed against many different proteins for therapeutical and analytical purposes[43,44]. Their use is shown here as attachment points for paramagnetic tags to analyze sensitive proteins like GPCRs, which by themselves would not support attachment of the labels without loss of function or structure. The Nb80 and Nb60 PCS tensors determined for the β_1AR complexes should be directly transferrable to β_2AR complexes, since β_1AR and β_2AR share very high similarity in their sequences and binding epitopes for both nanobodies. As the tagging sites reside in the conserved main scaffold of the nanobody and not in the complementarity-determining regions that recognize the specific epitope[45,46], the determined DOTA tagging sites, which provide large PCS values, can also be transferred across nanobodies. This is evident from the successful transfer of the sites from Nb80 to Nb60. We anticipate that these tagging sites can also be transferred to other nanobodies, such as Nb6, which has recently been introduced as an universal tool to determine the structures of many different GPCRs in their inactive state[47].

A further option may be to derive the PCS tensors from the nanobody resonances, instead of the GPCR resonances, with the goal that the tensors could be used universally for various recognized proteins. However, this approach may suffer from extensive line broadening due to PREs as well as from additional mobility between the nanobody and the recognized protein. Current efforts are directed to clarify these questions.

Nanobodies, which are single-domain antibodies derived from llamas, have a molecular weight of only 12–15 kDa and do not significantly increase the overall ~100 kDa size of the detergent-solubilized GPCR and consequently the NMR linewidths. Depending on the total size

of the antibody complex, it may however be even possible to use single-chain variable antibody fragments with sizes of ~25 kDa and still achieve reasonable spectral quality. It should also be noted that the present β_1AR was produced in insect cells in non-deuterated form and the NMR observations were carried out on ^{1}H-^{15}N backbone resonances. Considerably higher molecular weights as large as 1 MDa are reachable by perdeuteration and observation of ^{1}H-^{13}C methyl resonances[48].

The GPS-PCS method is not limited to antibodies obtained by immunization, but can also be used with any other stable biomacromolar binder. Thus the ultrastable, designed ankyrin repeat proteins (DARPins, 14–18 kDa) with affinities to the client protein in the picomolar range[49] seem ideally suited for DOTA tagging since they are very easily produced and do not contain any disulfide bond. GPS-PCS may also be extended to protein-nucleic acid complexes with either the protein or the nucleic tagged by DOTA[50]. Considering GPCRs, it is conceivable to also introduce DOTA tags into the engineered miniG transducer proteins[51], which could enable assignment of entire GPCR families in the active state. However, the stability of the miniG proteins under DOTA tagging and of the respective detergent-solubilized GPCR complexes remains to be investigated.

Experimental/Methods

Protein expression and purification

Expression of ^{15}N-valine-labeled YY-β_1AR in baculovirus-infected Sf9 cells (Oxford Expression Technologies) and receptor purification were carried out as described previously[15]. ^{15}N-tyrosine-labeled YY-β_1AR was expressed in a similar manner, but using custom-made serum-free medium (SF4, BioConcept) devoid of tyrosine and yeast extract, to which 75 mg/L ^{15}N-tyrosine were supplemented.

The original plasmids for Nb80/Nb60 were obtained from Jan Steyaert. Cysteine point mutations were introduced to both nanobodies through PCR using Phusion™ DNA Polymerase (Thermo Scientific). Nb80/Nb60 and their mutants were expressed in *E. coli* strain WK6 and purified according to the published protocol[52].

Site-specific labelling of single-cysteine nanobody mutants by Tm-DOTA-M7PT

Site-specific labeling of the single-cysteine nanobody mutants with Tm-DOTA-M7PT was performed according to the following procedure exemplified for the mutant Nb80-D108C. A strock solution of Tris(2-carboxyethyl)phosphine (TCEP) in base buffer (20 mM Tris, 100 mM NaCl, pH 7.5) was added to 2 mL 188 µM nanobody (5.2 mg) in the same buffer to reach a 2:1 molar TCEP:nanobody ratio. The solution was incubated overnight at 4 °C to reduce cysteine-glutathione disulfide bonds acquired during *E. coli* expression. The buffer was then exchanged to tagging buffer (20 mM Tris, 100 mM NaCl, 0.2 mM TCEP, pH 7.5) using a 10-kDa cut-off Amicon Ultra centrifugal concentrator (Merck Millipore) to reach nanobody concentration of 200 µM. A 4.5-fold molar excess of Tm-DOTA-M7PT (15 mM in acetonitrile) was then added to the solution and incubated in a PCMT Thermo-Shaker (Grant Instruments, Cambridge, UK) at 25 °C and 700 rpm until the conversion had reached 95% as monitored by high-resolution time-of-flight mass spectrometry (HR-TOF-MS, Figure S3) on a maXis 4G instrument (Bruker, Billerica, USA, accuracy ±1 Da). Reaction times varied between 5 and 64 hours (Table S1) apparently depending on the accessibility of individual cysteines. After the reaction, excess Tm-DOTA-M7PT was removed from the tagged nanobody by exchanging with base buffer using a 10-kDa cut-off Amicon Ultra centrifugal concentrator (Merck Millipore). For NMR, nanobodies were then concentrated to a final concentration of about 2 mM using 10-kDa cut-off Vivaspin centrifugal concentrators (Sartorius).

NMR experiments

NMR samples were prepared at a receptor concentration of 90−130 µM in 20 mM Tris, 100 mM NaCl, 0.1% DM, 5% D_2O, pH 7.5 (NMR buffer). The isoprenaline·YY-β_1AR complex was formed by adding 1 mM isoprenaline and 2 mM sodium ascorbate to the unliganded receptor.

To form the ternary active complex, a 1.2-molar equivalent of wild-type Nb80 or a 1.5-molar equivalent of Tm-DOTA-M7PT-tagged Nb80 cysteine mutants were added to the isoprenaline·YY-β_1AR complex. The sample of the ternary active complex was afterwards recycled through ligand exchange by competing out isoprenaline against carvedilol and releasing Nb80 to obtain the carvedilol·β_1AR complex. For this, the sample was washed three times with NMR buffer containing 200 µM carvedilol at tenfold dilution in an Amicon Ultra 50-kDa cutoff concentrator with 30 min incubation intervals. Wild-type Nb60 or Tm-DOTA-M7PT-tagged Nb60 cysteine mutants were then added to the carvedilol·YY-β_1AR complex at 1.2 and 1.5-molar ratios, respectively, to form carvedilol·YY-β_1AR·Nb60 complexes.

NMR experiments were performed on a Bruker AVANCE 900 MHz spectrometer equipped with a TCI cryogenic probe at 304 K using sample volumes of ~270 µL in 5-mm Shigemi microtubes. 2D ^{1}H-^{15}N TROSY spectra were recorded as 80 (^{15}N) x 1024 (^{1}H) complex points and acquisition periods of 16 ms (^{15}N) and 43 ms (^{1}H), with total experimental times of 24-48 h for non-paramagnetic samples and 58-72 h for paramagnetic samples. For optimal sensitivity, the ^{1}H-^{15}N INEPT transfer time was set to 3 ms to reduce magnetization losses from relaxation.

All NMR data were processed with the NMRpipe software package [53]. Spectra were displayed and analyzed with the program SPARKY[54].

Generation of β_1AR·Nb atom coordinates for structural analysis

For structural analysis of the isoprenaline·β_1AR·Nb80 complex in the active conformation, the coordinates were taken from the isoprenaline·β_1AR·Nb80 structure (PDB 6h7j, chain A/C). A structural model of the carvedilol·β_1AR·Nb60 complex in the inactive conformation was generated from the carazolol·β_2AR·Nb60 complex structure (PDB 5jqh) using its Nb60 coordinates (chain C) and replacing β_2AR (chain A) with β_1AR (chain A, PDB 4amj) via the PyMOL[55] alignment procedure. Hydrogens were added to both structures using MolProbity[56].

Tm-DOTA-M7PT-cysteine rotamer clash analysis

Coordinates of the Tm-DOTA-M7PT molecule were obtained by DFT calculations as described[27]. This molecule was then fitted by PyMOL[55] onto a standard cysteine residue at the corresponding C^{β}-S^{γ} bond and merged to form the Tm-DOTA-M7PT-cysteine residue (Figure 1A). A set 18 staggered side chain rotamers of this residue was then created within PyMOL by setting the respective angles $\chi_{1/2} = \pm 60^{\circ}$, 180° and $\chi_3 = \pm 90$. Each of these rotamers was then moved consecutively onto the residues of the target protein of interest (Nb) by superimposing the N, C^{α}, and C' backbone atoms using a Python script. Steric clashes were then calculated as the sum of the van der Waals penetrations $\Sigma_{vdwp} = \Sigma_{A,B}\, p_{AB}$ of all atom pairs A, B from the sidechain of the DOTA-cysteine residue and the target protein. The individual penetrations p_{AB}

of the two atoms are set to $p_{AB} = (R_{vdw,A}+R_{vdw,B}) - r_{AB}$ if $r_{AB} < (R_{vdw,A}+R_{vdw,B})$ and 0 otherwise, where $R_{vdw,A/B}$ represent the atoms' van der Waals radii and r_{AB} their distance. A very crude probability p_i of an individual side chain rotamer i was obtained as $p_i = A \exp(-\Sigma_{vdwp,i}/kT)$ using a fictive thermal energy kT and the normalization constant A derived from the condition $\Sigma_i p_i = 1$. Tests in the range kT = 5–100 Å showed that a value kT = 30 Å provided reasonable rotamer distributions, i.e. not too tight for larger side chain crevices at the surface, but more constrained for narrower crevices. These probabilities were then used to obtain an estimate for the averaged position of the paramagnetic Tm center $\langle \vec{R}_{TM} \rangle = \sum_i p_i \vec{R}_{TM,i}$.

Fitting of the PCS tensor by SVD

The PCS tensors were obtained from the measured PCS values (relative to a wild-type Nb complex), the estimated averaged position of the paramagnetic Tm center $\langle \vec{R}_{TM} \rangle$, and the Nb complex coordinates by least-squares fitting with singular value decomposition (SVD) implemented in Python using the described linear equations[57,58]. The tensor parameters were then outputted with the Euler angle Paramagpy[57] convention by using its subroutines (Supplementary Table S2) and visualized by PyMOL[55].

Solution of the best-matching assignment permutation problem

To obtain the best-matching assignment for a set of N NMR resonances and measured PCS values to the theoretical PCS values of the respective N nuclei, an N x N cost matrix C was generated containing the χ^2 differences between measured and theoretical values as $C_{ij} = [PCS_{meas}(\text{resonance } i) - PCS_{theo}(\text{nucleus } j)]^2$ (Figure 2G). The best best-matching assignment is then given as the permutation matrix P_{min} of all resonances, which minimize trace($P \cdot C$). A solution to this problem, which is efficient even for large N, was recently described using a simple, linear programing approach[31]. This approach was implemented using SciPy[59].

Figure legends

Figure 1. Rational selection of DOTA labeling sites from steric constraints on side chain rotamers. (A) Chemical structure of Tm-DOTA-M7PT-cysteine residue with side chain rotamer angles $\chi_{1\text{-}3}$. (B) Left: superimposed stick models of the 18 possible side chain rotamers of Tm-DOTA-M7PT-cysteine. The cysteine backbone heavy atoms are shown as spheres. Right: Tm-DOTA-M7PT-cysteine side chain rotamers superimposed onto residue position T57 of Nb80 (PDB 6h7j). The two rotamers with the smallest steric clashes ($\Sigma_{vdwp} < 30$ Å) are shown as solid, colored sticks, the other rotamers with significant steric clashes as grey transparent sticks, and the remainder of Nb80 as transparent spheres. (C) Count of rotamers of an individual Nb80 residue, for which the van der Waals clash sum (Σ_{vdwp}) are smaller than 60 Å, plotted against the minimal van der Waals clash sum (min. Σ_{vdwp}) of all rotamers for the respective residue (left) and against the rms of the observed PCS values of the $^{1}H^{N}$ valine resonances in YY-β_1AR. (D) Positions of residues in Nb80 that were tested for DOTA tagging by cysteine mutations. The residues are shown as green spheres within the β_1AR·Nb80 complex structure (PDB 6h7j).

Figure 2. Detection of PCSs induced by three different Nb80-DOTA variants on YY-β_1AR valine residues and automated assignment procedure of respective ^{1}H-^{15}N resonances. (A) Left: structure of β_1AR·Nb80 complex (PDB 6h7j). Valines are shown as blue spheres within β_1AR. Right: positions of Tm-DOTA-M7PT-cysteine residues (spheres) in the Nb80-Q39C/T57C/D108C variants that induced strong PCSs within YY-β_1AR (only one sidechain rotamer is shown). (B–D) ^{1}H-^{15}N TROSY spectra of ^{15}N-valine isoprenaline·YY-β_1AR in complexes with the Nb80-DOTA variants (colored) shown in (A) superimposed onto the spectrum of isoprenaline·YY-β_1AR in complex with wild-type Nb80 (black). (E) Superpositions of ^{1}H-^{15}N resonance positions of the spectra shown in (B–D) marked by the assigned valine residue numbers. (F) Algorithm for automated assignment of all 28 ^{1}H-^{15}N valine YY-β_1AR resonances based on PCS observations from several DOTA sites and 6 initial assignments. (G) Illustration of assignment cost matrix. (H) Evolution of the YY-β_1AR valine assignments during the automated assignment algorithm. (I) Evolution of the PCS tensors for the three Nb80-DOTA variants during the automated assignment algorithm. Solid lines depict the amplitudes of the tensors relative to their final values obtained from all 28 assignments. Dashed lines depict the directional cosines of the tensors relative to their final values. (J) Predicted vs experimental ^{1}H valine YY-β_1AR PCS values for the three different Nb80-DOTA variants according to the final assignments and tensor values. The spatial distributions of the PCS tensors within the β_1AR·Nb80 complex structures are shown on the right. Positive (blue) and negative (red) isosurfaces indicate a PCS of 1.0/0.2 ppm (inner sphere/outer sphere). (K) Final assignment of ^{1}H-^{15}N valine resonances marked on the TROSY spectrum of the isoprenaline·YY-β_1AR·Nb80(wild-type) complex. The labels are color-coded as black for the 6 initially known assignments, blue for the additional 10 most well-resolved resonances, and red for the resonances in the crowded region of the spectrum.

Figure 3. NMR response of YY-β_1AR to antagonist, agonist and Nb80 binding. (A,B,C) ^{1}H-^{15}N TROSY spectra of ^{15}N-valine labeled YY-β_1AR complexed with antagonist carvedilol (A, magenta), full agonist isoprenaline (B, marine), and isoprenaline/Nb80 (C, orange) superimposed onto the spectrum of the apo state (black). Larger peak shifts are indicated by red

dashed lines. (D) Combined ^{1}H, ^{15}N chemical shift perturbations CSP of all 28 valine resonances observed in carvedilol- (magenta), isoprenaline- (marine), and isoprenaline/Nb80- (orange) bound forms relative to the apo form. (E) Structure of β_1AR in complex with isoprenaline (PDB 2y03). The protein backbone and isoprenaline are shown in ribbon and black stick representation, respectively. Individual valines are depicted as spheres. Red spheres indicate valines, for which resonances corresponding to both the preactive and active conformation are observed in the isoprenaline-bound state. These valines are also marked in (D) by red dots underneath the residue numbers. Valines, for which the active conformation could not (yet) be observed in the isoprenaline-bound state, are shown as blue spheres. Asterisks denote tentative assignments.

Figure 4. Global backbone perturbation of YY-β_1AR upon Nb80 binding. (A) ^{1}H-^{15}N TROSY spectrum of ^{15}N-valine YY-β_1AR complexed with isoprenaline and Nb80 (orange) superimposed onto spectrum of isoprenaline-bound ^{15}N-valine YY-β_1AR. Larger peak shifts are indicated as dashed lines, very large shifts (CSP > 0.5 ppm) are highlighted in red. (B) Localization of valines (red circles) with very large shifts (CSP > 0.5 ppm) within a schematic presentation of YY-β_1AR. (C,D) Structural changes and chemical shift difference of valines analyzed in individual transmembrane helices and loop regions of β_1AR. In (C), transmembrane helices of the isoprenaline·β_1AR complex structure (PDB 2y03, grey) are superimposed onto the helices of the isoprenaline·β_1AR·Nb80 complex structure (PDB 6h7j, colored). Backbone nitrogens of valines are shown as spheres in red (CSP > 0.5 ppm), orange (0.1 < CSP < 0.5 ppm) and grey (CSP < 0.1 ppm). Asterisks denote tentative assignments.

Figure 5. Application of the GPS-PCS method to the assignment of ^{15}N-tyrosines in YY-β_1AR. (A) ^{1}H-^{15}N TROSY spectra of ^{15}N-tyrosine labeled isoprenaline·YY-β_1AR in complexes with paramagnetic Tm-DOTA-M7PT-tagged Nb80-Q39C (blue) and Nb80-T57C (green) as well as diamagnetic wild-type Nb80. The PCSs are indicated by solid red lines, except for Y149 (marked by asterisk), for which the paramagnetic-shifted resonances were not observed. Resonances marked by 'i' originate from an unidentified low-molecular weight impurity and were insensitive to paramagnetic shifts. (B) Experimental $^{1}H^{N}$ PCSs of the tyrosine residues versus $^{1}H^{N}$ PCSs predicted using the PCS tensors obtained from the valine assignments. (C) ^{1}H-^{15}N TROSY spectra of ^{15}N-tyrosine labeled YY-β_1AR in complex with antagonist carvedilol (magenta) and full agonist isoprenaline (marine). The Y333 resonances are connected by a black dashed line to highlight the shift from the inactive to the preactive state, as well as the coexistence of the preactive (p) and active (a) conformation of the isoprenaline·YY-β_1AR complex. (D) ^{1}H-^{15}N TROSY spectra of ^{15}N-tyrosine labeled YY-β_1AR in complex with agonist isoprenaline (marine), and both isoprenaline and Nb80 (orange). Larger peak shifts are indicated as dashed lines, particularly large shifts (CSP > 0.25 ppm) are highlighted in red. (E) CSP analysis of all 9 tyrosine ^{1}H-^{15}N resonances in YY-β_1AR for the transition from the inactive (carvedilol complex) to the preactive (isoprenaline complex) conformation (marine) and from the preactive to the active (isoprenaline + Nb80 complex) conformation (orange). (F) Aligned structures of isoprenaline·β_1AR complex (PDB 2y03, marine), and isoprenaline·β_1AR·Nb80 complex (PDB 6h7j, orange). Backbone nitrogen atoms (spheres) and side chains (sticks) of tyrosines are shown in red (CSP > 0.25 ppm) and grey (CSP < 0.25 ppm).

Supporting Information

Supporting Figure and Tables: NMR spectra of Nb60-bound ^{15}N-valine and ^{15}N-tyrosine YY-β_1AR, mass spectra of Tm-DOTA-M7PT labeling reaction, labeling reaction times, parameters of fitted PCS tensors.

Acknowledgements

This work was supported by the Swiss National Science Foundation (31-149927, 31-173089, 31-201270 to S.G. and 31-179319 to A.D.G.). D.H. acknowledges financial support by the Department of Chemistry of the University of Basel. We gratefully acknowledge Dr. Jan Steyaert for the generous gift of the Nb80 and Nb60 plasmids as well as Dr. Thomas Müntener for very helpful discussions.

References

(1) Tugarinov, V.; Muhandiram, R.; Ayed, A.; Kay, L. Four-Dimensional NMR Spectroscopy of a 723-Residue Protein: Chemical Shift Assignments and Secondary Structure of Malate Synthase g. *J. Am. Chem. Soc.* **2002**, *124* (34), 10025–35x.

(2) Bertini, I.; Luchinat, C.; Parigi, G.; Pierattelli, R. NMR Spectroscopy of Paramagnetic Metalloproteins. *ChemBioChem* **2005**, *6* (9), 1536–1549. https://doi.org/10.1002/cbic.200500124.

(3) Pintacuda, G.; Keniry, M. A.; Huber, T.; Park, A. Y.; Dixon, N. E.; Otting, G. Fast Structure-Based Assignment of ^{15} N HSQC Spectra of Selectively ^{15} N-Labeled Paramagnetic Proteins. *J. Am. Chem. Soc.* **2004**, *126* (9), 2963–2970. https://doi.org/10.1021/ja039339m.

(4) John, M.; Schmitz, C.; Park, A. Y.; Dixon, N. E.; Huber, T.; Otting, G. Sequence-Specific and Stereospecific Assignment of Methyl Groups Using Paramagnetic Lanthanides. *J. Am. Chem. Soc.* **2007**, *129* (44), 13749–13757. https://doi.org/10.1021/ja0744753.

(5) Velyvis, A.; Schachman, H. K.; Kay, L. E. Assignment of Ile, Leu, and Val Methyl Correlations in Supra-Molecular Systems: An Application to Aspartate Transcarbamoylase. *J. Am. Chem. Soc.* **2009**, *131* (45), 16534–16543. https://doi.org/10.1021/ja906978r.

(6) Barthelmes, K.; Reynolds, A. M.; Peisach, E.; Jonker, H. R. A.; DeNunzio, N. J.; Allen, K. N.; Imperiali, B.; Schwalbe, H. Engineering Encodable Lanthanide-Binding Tags into Loop Regions of Proteins. *J. Am. Chem. Soc.* **2011**, *133* (4), 808–819. https://doi.org/10.1021/ja104983t.

(7) Su, X.-C.; Huber, T.; Dixon, N. E.; Otting, G. Site-Specific Labelling of Proteins with a Rigid Lanthanide-Binding Tag. *Chembiochem* **2006**, *7* (10), 1599–1604. https://doi.org/10.1002/cbic.200600142.

(8) Miao, Q.; Nitsche, C.; Orton, H.; Overhand, M.; Otting, G.; Ubbink, M. Paramagnetic Chemical Probes for Studying Biological Macromolecules. *Chem. Rev.* **2022**, *122* (10), 9571–9642. https://doi.org/10.1021/acs.chemrev.1c00708.

(9) Müntener, T.; Joss, D.; Häussinger, D.; Hiller, S. Pseudocontact Shifts in Biomolecular NMR Spectroscopy. *Chem. Rev.* **2022**, *122* (10), 9422–9467. https://doi.org/10.1021/acs.chemrev.1c00796.

(10) Häussinger, D.; Huang, J.; Grzesiek, S. DOTA-M8: An Extremely Rigid, High-Affinity Lanthanide Chelating Tag for PCS NMR Spectroscopy. *J. Am. Chem. Soc.* **2009**, *131* (41), 14761–14767. https://doi.org/10.1021/ja903233w.

(11) Keizers, P.; Desreux, J.; Overhand, M.; Ubbink, M. Increased Paramagnetic Effect of a Lanthanide Protein Probe by Two-Point Attachment. *J. Am. Chem. Soc.* **2007**, *129* (30), 9292–9293.

(12) Alexander, S. P.; Christopoulos, A.; Davenport, A. P.; Kelly, E.; Marrion, N. V.; Peters, J. A.; Faccenda, E.; Harding, S. D.; Pawson, A. J.; Sharman, J. L.; Southan, C.; Davies, J. A.; CGTP Collaborators. THE CONCISE GUIDE TO PHARMACOLOGY 2017/18: G Protein-Coupled Receptors. *Br. J. Pharmacol.* **2017**, *174 Suppl 1* (Suppl Suppl 1), S17–S129. https://doi.org/10.1111/bph.13878.

(13) Eddy, M. T.; Lee, M.-Y.; Gao, Z.-G.; White, K. L.; Didenko, T.; Horst, R.; Audet, M.; Stanczak, P.; McClary, K. M.; Han, G. W.; Jacobson, K. A.; Stevens, R. C.; Wüthrich, K. Allosteric Coupling of Drug Binding and Intracellular Signaling in the A2A Adenosine Receptor. *Cell* **2018**, *172* (1–2), 68-80.e12. https://doi.org/10.1016/j.cell.2017.12.004.

(14) Grahl, A.; Abiko, L. A.; Isogai, S.; Sharpe, T.; Grzesiek, S. A High-Resolution Description of B1-Adrenergic Receptor Functional Dynamics and Allosteric Coupling from Backbone NMR. *Nat. Commun.* **2020**, *11* (1), 2216. https://doi.org/10.1038/s41467-020-15864-y.

(15) Isogai, S.; Deupi, X.; Opitz, C.; Heydenreich, F. M.; Tsai, C.-J.; Brueckner, F.; Schertler, G. F. X.; Veprintsev, D. B.; Grzesiek, S. Backbone NMR Reveals Allosteric Signal Transduction Networks in the B1-Adrenergic Receptor. *Nature* **2016**, *530* (7589), 237–241. https://doi.org/10.1038/nature16577.

(16) Kofuku, Y.; Ueda, T.; Okude, J.; Shiraishi, Y.; Kondo, K.; Maeda, M.; Tsujishita, H.; Shimada, I. Efficacy of the B2-Adrenergic Receptor Is Determined by Conformational Equilibrium in the Transmembrane Region. *Nat. Commun.* **2012**, *3* (1), 1045. https://doi.org/10.1038/ncomms2046.

(17) Latorraca, N. R.; Venkatakrishnan, A. J.; Dror, R. O. GPCR Dynamics: Structures in Motion. *Chem. Rev.* **2017**, *117* (1), 139–155. https://doi.org/10.1021/acs.chemrev.6b00177.

(18) Liu, J. J.; Horst, R.; Katritch, V.; Stevens, R. C.; Wüthrich, K. Biased Signaling Pathways in B2-Adrenergic Receptor Characterized by 19F-NMR. *Science* **2012**, *335* (6072), 1106–1110. https://doi.org/10.1126/science.1215802.

(19) Manglik, A.; Kobilka, B. The Role of Protein Dynamics in GPCR Function: Insights from the B2AR and Rhodopsin. *Curr. Opin. Cell Biol.* **2014**, *27*, 136–143. https://doi.org/10.1016/j.ceb.2014.01.008.

(20) Okude, J.; Ueda, T.; Kofuku, Y.; Sato, M.; Nobuyama, N.; Kondo, K.; Shiraishi, Y.; Mizumura, T.; Onishi, K.; Natsume, M.; Maeda, M.; Tsujishita, H.; Kuranaga, T.; Inoue, M.; Shimada, I. Identification of a Conformational Equilibrium That Determines the Efficacy and Functional Selectivity of the μ-Opioid Receptor. *Angew. Chem. Int. Ed.* **2015**, *54* (52), 15771–15776. https://doi.org/10.1002/anie.201508794.

(21) Rößler, P.; Mayer, D.; Tsai, C.-J.; Veprintsev, D. B.; Schertler, G. F. X.; Gossert, A. D. GPCR Activation States Induced by Nanobodies and Mini-G Proteins Compared by NMR Spectroscopy. *Molecules* **2020**, *25* (24), 5984. https://doi.org/10.3390/molecules25245984.

(22) Solt, A. S.; Bostock, M. J.; Shrestha, B.; Kumar, P.; Warne, T.; Tate, C. G.; Nietlispach, D. Insight into Partial Agonism by Observing Multiple Equilibria for Ligand-Bound and Gs-Mimetic Nanobody-Bound B1-Adrenergic Receptor. *Nat. Commun.* **2017**, *8* (1), 1795. https://doi.org/10.1038/s41467-017-02008-y.
(23) Wu, F.-J.; Williams, L. M.; Abdul-Ridha, A.; Gunatilaka, A.; Vaid, T. M.; Kocan, M.; Whitehead, A. R.; Griffin, M. D. W.; Bathgate, R. A. D.; Scott, D. J.; Gooley, P. R. Probing the Correlation between Ligand Efficacy and Conformational Diversity at the A1A-Adrenoreceptor Reveals Allosteric Coupling of Its Microswitches. *J. Biol. Chem.* **2020**, *295* (21), 7404–7417. https://doi.org/10.1074/jbc.RA120.012842.
(24) Ye, L.; Van Eps, N.; Zimmer, M.; Ernst, O. P.; Scott Prosser, R. Activation of the A2A Adenosine G-Protein-Coupled Receptor by Conformational Selection. *Nature* **2016**, *533* (7602), 265–268. https://doi.org/10.1038/nature17668.
(25) Abiko, L. A.; Grahl, A.; Grzesiek, S. High Pressure Shifts the B1-Adrenergic Receptor to the Active Conformation in the Absence of g Protein. *J. Am. Chem. Soc.* **2019**, *141* (42), 16663–16670. https://doi.org/10.1021/jacs.9b06042.
(26) Rasmussen, S. G. F.; DeVree, B. T.; Zou, Y.; Kruse, A. C.; Chung, K. Y.; Kobilka, T. S.; Thian, F. S.; Chae, P. S.; Pardon, E.; Calinski, D.; Mathiesen, J. M.; Shah, S. T. A.; Lyons, J. A.; Caffrey, M.; Gellman, S. H.; Steyaert, J.; Skiniotis, G.; Weis, W. I.; Sunahara, R. K.; Kobilka, B. K. Crystal Structure of the B2 Adrenergic Receptor–Gs Protein Complex. *Nature* **2011**, *477* (7366), 549–555. https://doi.org/10.1038/nature10361.
(27) Müntener, T.; Kottelat, J.; Huber, A.; Häussinger, D. New Lanthanide Chelating Tags for PCS NMR Spectroscopy with Reduction Stable, Rigid Linkers for Fast and Irreversible Conjugation to Proteins. *Bioconjug. Chem.* **2018**, *29* (10), 3344–3351. https://doi.org/10.1021/acs.bioconjchem.8b00512.
(28) Rasmussen, S. G. F.; Choi, H.-J.; Fung, J. J.; Pardon, E.; Casarosa, P.; Chae, P. S.; DeVree, B. T.; Rosenbaum, D. M.; Thian, F. S.; Kobilka, T. S.; Schnapp, A.; Konetzki, I.; Sunahara, R. K.; Gellman, S. H.; Pautsch, A.; Steyaert, J.; Weis, W. I.; Kobilka, B. K. Structure of a Nanobody-Stabilized Active State of the B2 Adrenoceptor. *Nature* **2011**, *469* (7329), 175–180. https://doi.org/10.1038/nature09648.
(29) Warne, T.; Edwards, P. C.; Doré, A. S.; Leslie, A. G. W.; Tate, C. G. Molecular Basis for High-Affinity Agonist Binding in GPCRs. *Sci. N. Y. NY* **2019**, *364* (6442), 775–778. https://doi.org/10.1126/science.aau5595.
(30) Ballesteros, J. A.; Weinstein, H. [19] Integrated Methods for the Construction of Three-Dimensional Models and Computational Probing of Structure-Function Relations in G Protein-Coupled Receptors. In *Methods in Neurosciences*; Sealfon, S. C., Ed.; Receptor Molecular Biology; Academic Press, 1995; Vol. 25, pp 366–428. https://doi.org/10.1016/S1043-9471(05)80049-7.
(31) Collier, O.; Dalalyan, A. S. Minimax Rates in Permutation Estimation for Feature Matching. *J. Mach. Learn. Res.* **2016**, *17* (1), 162–192.
(32) Staus, D. P.; Strachan, R. T.; Manglik, A.; Pani, B.; Kahsai, A. W.; Kim, T. H.; Wingler, L. M.; Ahn, S.; Chatterjee, A.; Masoudi, A.; Kruse, A. C.; Pardon, E.; Steyaert, J.; Weis, W. I.; Prosser, R. S.; Kobilka, B. K.; Costa, T.; Lefkowitz, R. J. Allosteric Nanobodies Reveal the Dynamic Range and Diverse Mechanisms of G-Protein-Coupled Receptor Activation. *Nature* **2016**, *535* (7612), 448–452. https://doi.org/10.1038/nature18636.
(33) Grzesiek, S.; Cordier, F.; Jaravine, V.; Barfield, M. Insights into Biomolecular Hydrogen Bonds from Hydrogen Bond Scalar Couplings. *Prog. Nucl. Magn. Reson. Spectrosc.* **2004**, *45* (3–4), 275–300.
(34) Xu, X.-P.; Case, D. A. Probing Multiple Effects on 15N, 13C Alpha, 13C Beta, and 13C' Chemical Shifts in Peptides Using Density Functional Theory. *Biopolymers* **2002**, *65* (6), 408–423. https://doi.org/10.1002/bip.10276.
(35) Scheerer, P.; Park, J. H.; Hildebrand, P. W.; Kim, Y. J.; Krauss, N.; Choe, H.-W.; Hofmann, K. P.; Ernst, O. P. Crystal Structure of Opsin in Its G-Protein-Interacting Conformation. *Nature* **2008**, *455* (7212), 497–502. https://doi.org/10.1038/nature07330.
(36) Hauser, A. S.; Kooistra, A. J.; Munk, C.; Heydenreich, F. M.; Veprintsev, D. B.; Bouvier, M.; Babu, M. M.; Gloriam, D. E. GPCR Activation Mechanisms across Classes and Macro/Microscales. *Nat. Struct. Mol. Biol.* **2021**, *28* (11), 879–888. https://doi.org/10.1038/s41594-021-00674-7.
(37) Venkatakrishnan, A. J.; Deupi, X.; Lebon, G.; Tate, C. G.; Schertler, G. F.; Babu, M. M. Molecular Signatures of G-Protein-Coupled Receptors. *Nature* **2013**, *494* (7436), 185–194. https://doi.org/10.1038/nature11896.
(38) Cherezov, V.; Rosenbaum, D. M.; Hanson, M. A.; Rasmussen, S. G. F.; Thian, F. S.; Kobilka, T. S.; Choi, H.-J.; Kuhn, P.; Weis, W. I.; Kobilka, B. K.; Stevens, R. C. High-Resolution Crystal Structure of an Engineered Human Beta2-Adrenergic G Protein-Coupled Receptor. *Sci. N. Y. NY* **2007**, *318* (5854), 1258–1265. https://doi.org/10.1126/science.1150577.
(39) Ring, A. M.; Manglik, A.; Kruse, A. C.; Enos, M. D.; Weis, W. I.; Garcia, K. C.; Kobilka, B. K. Adrenaline-Activated Structure of B2-Adrenoceptor Stabilized by an Engineered Nanobody. *Nature* **2013**, *502* (7472), 575xEPx – 579. https://doi.org/10.1038/nature12572.
(40) Isaikina, P.; Tsai, C.-J.; Dietz, N.; Pamula, F.; Grahl, A.; Goldie, K. N.; Guixà-González, R.; Branco, C.; Paolini-Bertrand, M.; Calo, N.; Cerini, F.; Schertler, G. F. X.; Hartley, O.; Stahlberg, H.; Maier, T.; Deupi, X.; Grzesiek, S. Structural Basis of the Activation of the CC Chemokine Receptor 5 by a Chemokine Agonist. *Sci. Adv.* **2021**, *7* (25), eabg8685. https://doi.org/10.1126/sciadv.abg8685.

(41) Joss, D.; Winter, F.; Häussinger, D. A Novel, Rationally Designed Lanthanoid Chelating Tag Delivers Large Paramagnetic Structural Restraints for Biomolecular NMR. *Chem. Commun.* **2020**, *56* (84), 12861–12864. https://doi.org/10.1039/D0CC04337K.
(42) Kuhn, H. W. The Hungarian Method for the Assignment Problem. *Nav. Res. Logist. Q.* **1955**, *2* (1–2), 83–97. https://doi.org/10.1002/nav.3800020109.
(43) Bao, G.; Tang, M.; Zhao, J.; Zhu, X. Nanobody: A Promising Toolkit for Molecular Imaging and Disease Therapy. *EJNMMI Res.* **2021**, *11* (1), 6. https://doi.org/10.1186/s13550-021-00750-5.
(44) Hamers-Casterman, C.; Atarhouch, T.; Muyldermans, S.; Robinson, G.; Hammers, C.; Songa, E. B.; Bendahman, N.; Hammers, R. Naturally Occurring Antibodies Devoid of Light Chains. *Nature* **1993**, *363* (6428), 446–448. https://doi.org/10.1038/363446a0.
(45) Manglik, A.; Kobilka, B. K.; Steyaert, J. Nanobodies to Study G Protein–Coupled Receptor Structure and Function. *Annu. Rev. Pharmacol. Toxicol.* **2017**, *57* (1), 19–37. https://doi.org/10.1146/annurev-pharmtox-010716-104710.
(46) McMahon, C.; Baier, A. S.; Pascolutti, R.; Wegrecki, M.; Zheng, S.; Ong, J. X.; Erlandson, S. C.; Hilger, D.; Rasmussen, S. G. F.; Ring, A. M.; Manglik, A.; Kruse, A. C. Yeast Surface Display Platform for Rapid Discovery of Conformationally Selective Nanobodies. *Nat. Struct. Mol. Biol.* **2018**, *25* (3), 289–296. https://doi.org/10.1038/s41594-018-0028-6.
(47) Robertson, M. J.; Papasergi-Scott, M.; He, F.; Seven, A. B.; Meyerowitz, J. G.; Panova, O.; Peroto, M. C.; Che, T.; Skiniotis, G. *Structure Determination of Inactive-State GPCRs with a Universal Nanobody*; preprint; Biophysics, 2021. https://doi.org/10.1101/2021.11.02.466983.
(48) Rosenzweig, R.; Kay, L. E. Bringing Dynamic Molecular Machines into Focus by Methyl-TROSY NMR. *Annu. Rev. Biochem.* **2014**, *83* (1), 291–315. https://doi.org/10.1146/annurev-biochem-060713-035829.
(49) Plückthun, A. Designed Ankyrin Repeat Proteins (DARPins): Binding Proteins for Research, Diagnostics, and Therapy. *Annu. Rev. Pharmacol. Toxicol.* **2015**, *55* (1), 489–511. https://doi.org/10.1146/annurev-pharmtox-010611-134654.
(50) Joss, D.; Häussinger, D. Design and Applications of Lanthanide Chelating Tags for Pseudocontact Shift NMR Spectroscopy with Biomacromolecules. *Prog. Nucl. Magn. Reson. Spectrosc.* **2019**, *114–115*, 284–312. https://doi.org/10.1016/j.pnmrs.2019.08.002.
(51) Nehmé, R.; Carpenter, B.; Singhal, A.; Strege, A.; Edwards, P. C.; White, C. F.; Du, H.; Grisshammer, R.; Tate, C. G. Mini-G Proteins: Novel Tools for Studying GPCRs in Their Active Conformation. *PLOS ONE* **2017**, *12* (4), e0175642. https://doi.org/10.1371/journal.pone.0175642.
(52) Pardon, E.; Laeremans, T.; Triest, S.; Rasmussen, S. G. F.; Wohlkönig, A.; Ruf, A.; Muyldermans, S.; Hol, W. G. J.; Kobilka, B. K.; Steyaert, J. A General Protocol for the Generation of Nanobodies for Structural Biology. *Nat. Protoc.* **2014**, *9* (3), 674–693. https://doi.org/10.1038/nprot.2014.039.
(53) Delaglio, F.; Grzesiek, S.; Vuister, G. W.; Zhu, G.; Pfeifer, J.; Bax, A. NMRPipe: A Multidimensional Spectral Processing System Based on UNIX Pipes. *J Biomol NMR* **1995**, *6* (3), 277–293. https://doi.org/10.1007/bf00197809.
(54) Lee, W.; Tonelli, M.; Markley, J. L. NMRFAM-SPARKY: Enhanced Software for Biomolecular NMR Spectroscopy. *Bioinformatics* **2015**, *31* (8), 1325–1327. https://doi.org/10.1093/bioinformatics/btu830.
(55) *PyMOL | pymol.org*. The PyMOL Molecular Graphics System, Version 2.3.0, Schrödinger, LLC. https://pymol.org/2/ (accessed 2020-07-19).
(56) Williams, C. J.; Headd, J. J.; Moriarty, N. W.; Prisant, M. G.; Videau, L. L.; Deis, L. N.; Verma, V.; Keedy, D. A.; Hintze, B. J.; Chen, V. B.; Jain, S.; Lewis, S. M.; Arendall III, W. B.; Snoeyink, J.; Adams, P. D.; Lovell, S. C.; Richardson, J. S.; Richardson, D. C. MolProbity: More and Better Reference Data for Improved All-Atom Structure Validation. *Protein Sci.* **2018**, *27* (1), 293–315. https://doi.org/10.1002/pro.3330.
(57) Orton, H. W.; Huber, T.; Otting, G. Paramagpy: Software for Fitting Magnetic Susceptibility Tensors Using Paramagnetic Effects Measured in NMR Spectra. *Magn. Reson.* **2020**, *1* (1), 1–12. https://doi.org/10.5194/mr-1-1-2020.
(58) Sass, J.; Cordier, F.; Hoffmann, A.; Cousin, A.; Omichinski, J.; Lowen, H.; Grzesiek, S. Purple Membrane Induced Alignment of Biological Macromolecules in the Magnetic Field. *J. Am. Chem. Soc.* **1999**, *121* (10), 2047–2055.
(59) Virtanen, P.; Gommers, R.; Oliphant, T. E.; Haberland, M.; Reddy, T.; Cournapeau, D.; Burovski, E.; Peterson, P.; Weckesser, W.; Bright, J.; van der Walt, S. J.; Brett, M.; Wilson, J.; Millman, K. J.; Mayorov, N.; Nelson, A. R. J.; Jones, E.; Kern, R.; Larson, E.; Carey, C. J.; Polat, İ.; Feng, Y.; Moore, E. W.; VanderPlas, J.; Laxalde, D.; Perktold, J.; Cimrman, R.; Henriksen, I.; Quintero, E. A.; Harris, C. R.; Archibald, A. M.; Ribeiro, A. H.; Pedregosa, F.; van Mulbregt, P. SciPy 1.0: Fundamental Algorithms for Scientific Computing in Python. *Nat. Methods* **2020**, *17* (3), 261–272. https://doi.org/10.1038/s41592-019-0686-2.

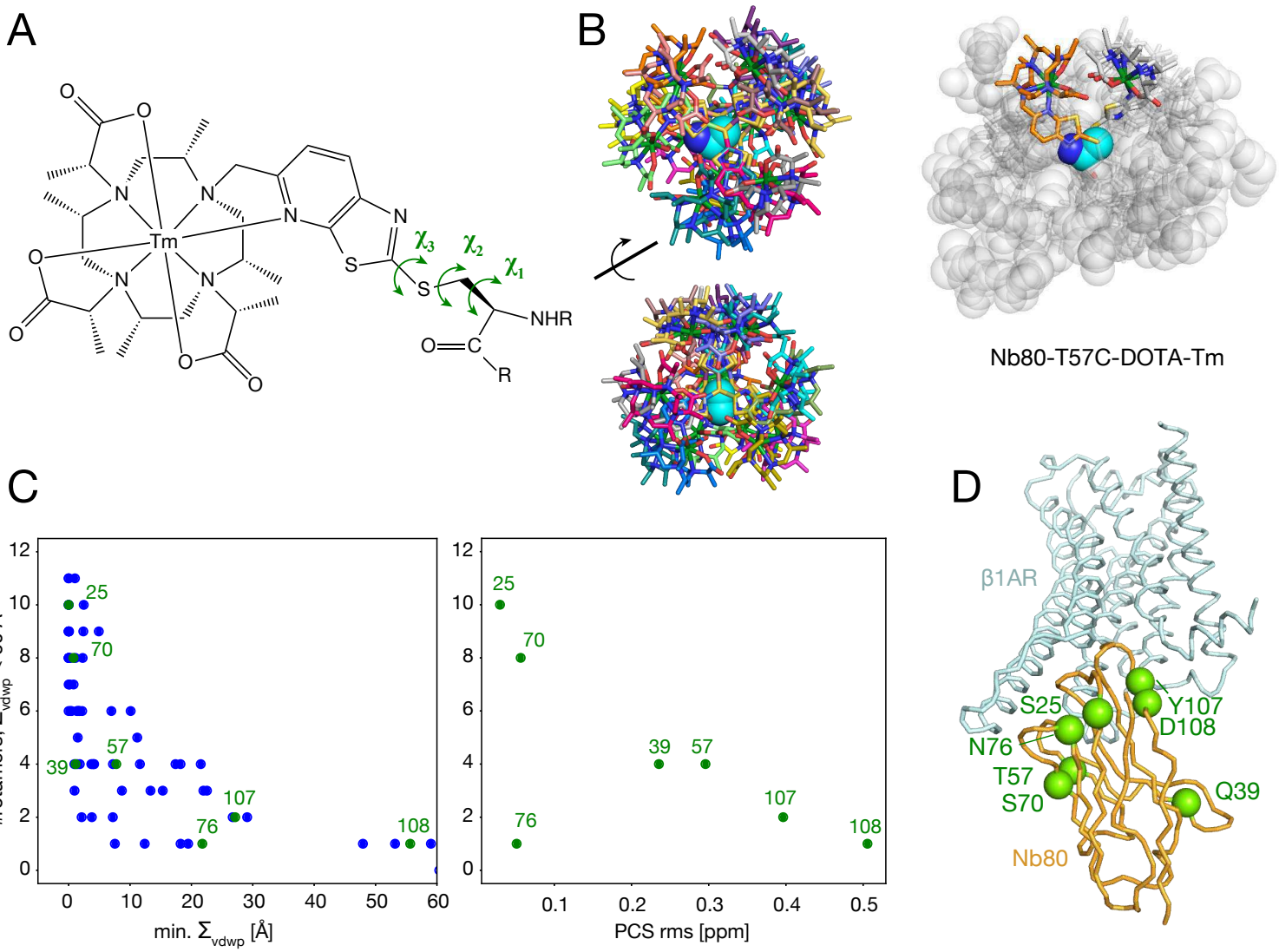
A
B
C
D
Tm
χ3
χ2
χ1
NHR
R
Nb80-T57C-DOTA-Tm
#rotamers, Σvdwp < 60 Å
min. Σvdwp [Å]
PCS rms [ppm]
25
70
39
57
107
76
108
β1AR
Nb80
S25
Y107
D108
N76
T57
S70
Q39

Figure 1

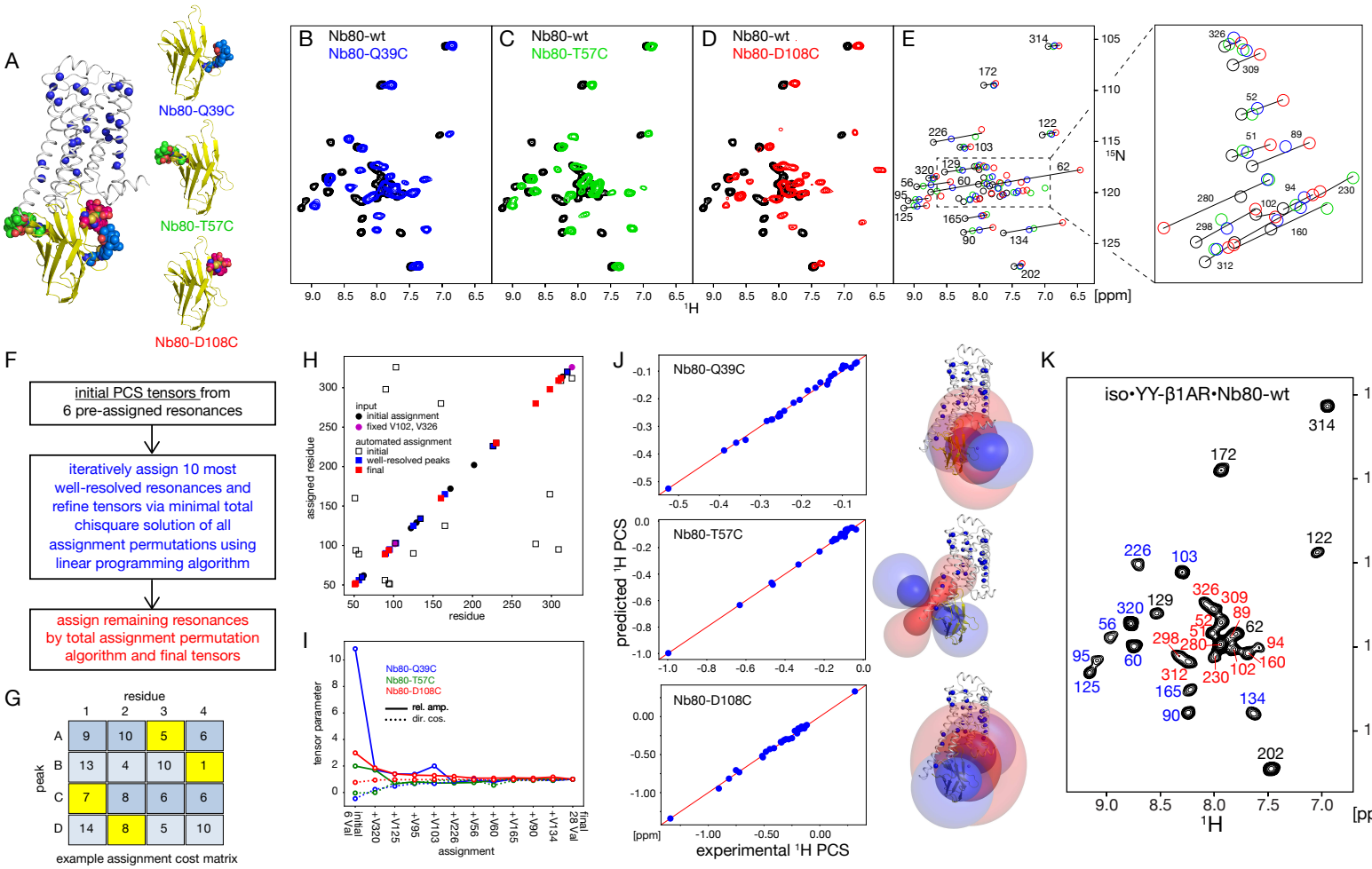

peak \ residue	1	2	3	4
A	9	10	5	6
B	13	4	10	1
C	7	8	6	6
D	14	8	5	10

Figure 2

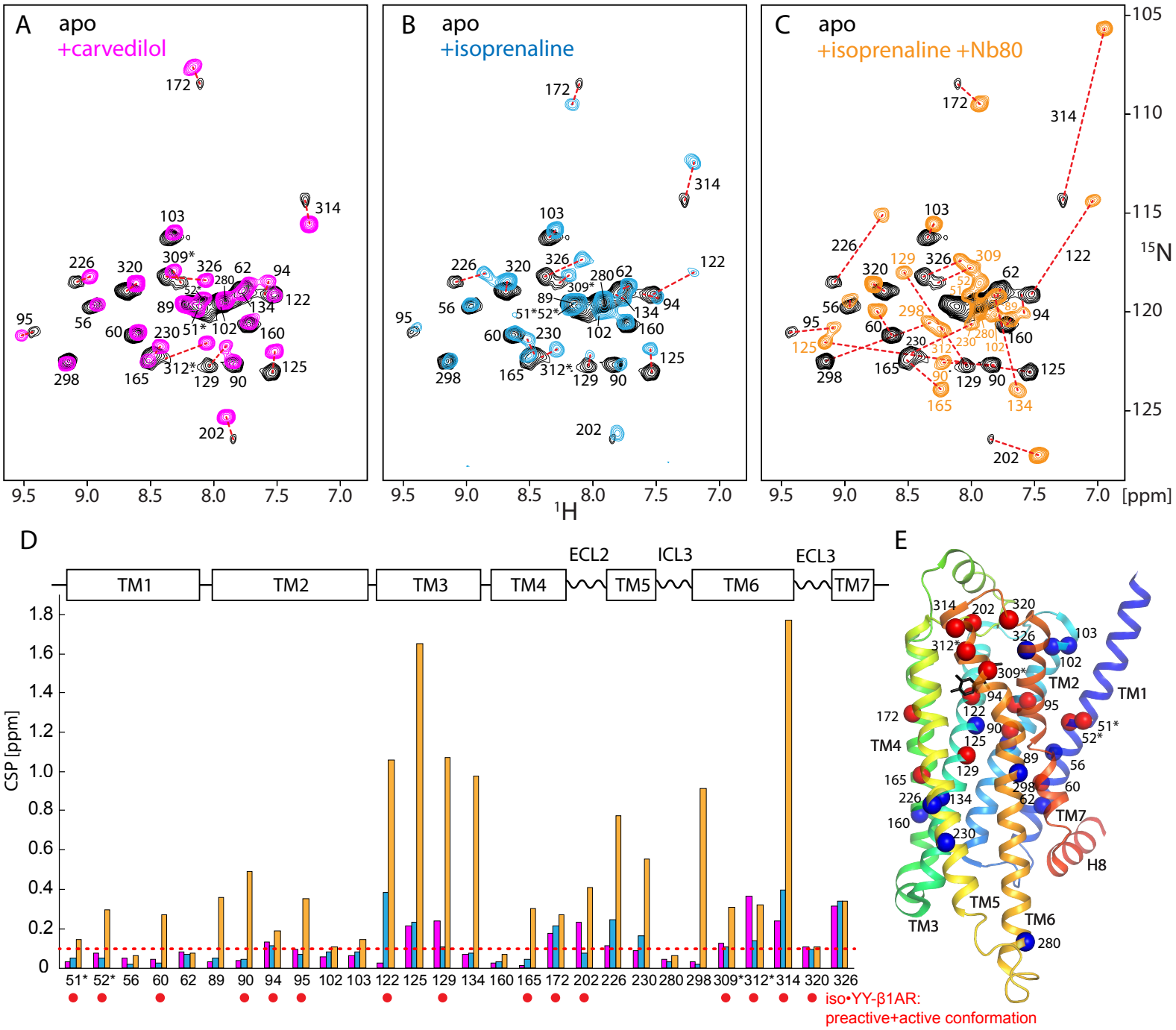
A
apo
+carvedilol
B
apo
+isoprenaline
C
apo
+isoprenaline +Nb80
^{15}N
^{1}H
[ppm]
D
TM1
TM2
TM3
TM4
ECL2
TM5
ICL3
TM6
ECL3
TM7
CSP [ppm]
iso•YY-β1AR:
preactive+active conformation
E
TM1
TM2
TM3
TM4
TM5
TM6
TM7
H8

Figure 3

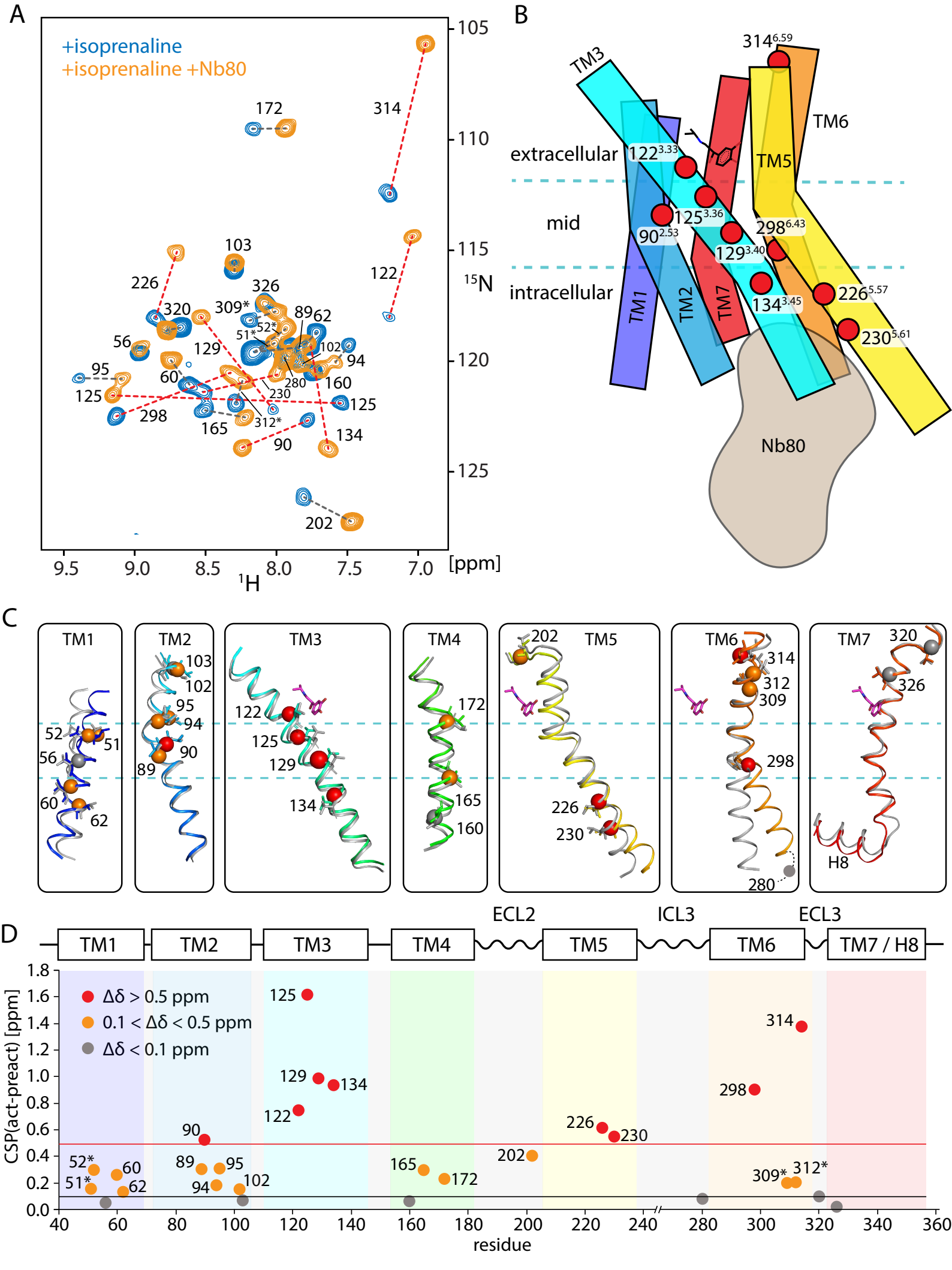
A
+isoprenaline
+isoprenaline +Nb80
105
110
115
120
125
15N
9.5
9.0
8.5
8.0
7.5
7.0
[ppm]
1H
B
TM3
TM6
TM5
TM1
TM2
TM7
extracellular
mid
intracellular
Nb80
C
TM1
TM2
TM3
TM4
TM5
TM6
TM7
H8
D
ECL2
ICL3
ECL3
TM1
TM2
TM3
TM4
TM5
TM6
TM7 / H8
Δδ > 0.5 ppm
0.1 < Δδ < 0.5 ppm
Δδ < 0.1 ppm
CSP(act-preact) [ppm]
residue

Figure 4

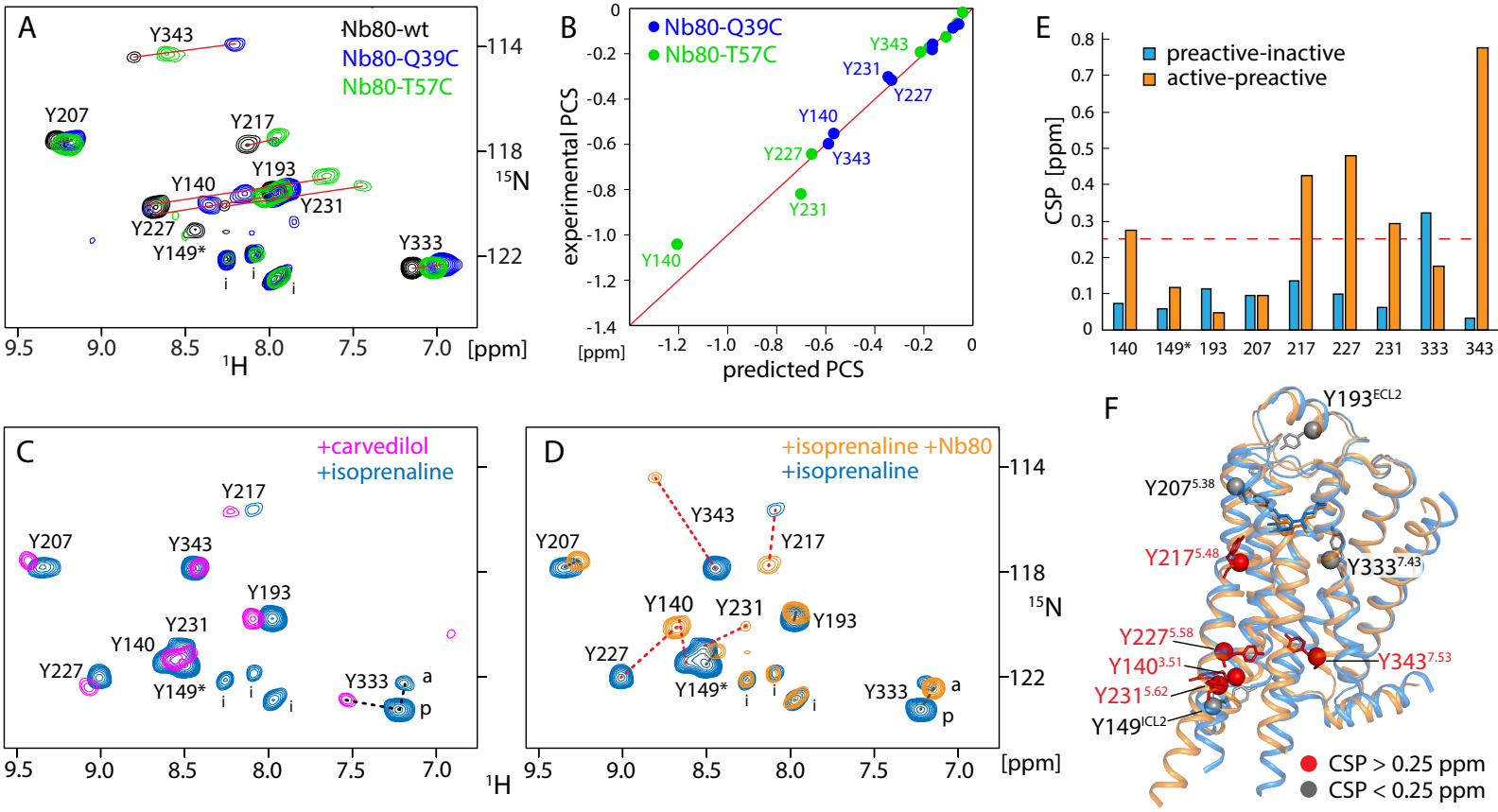
A
Nb80-wt
Nb80-Q39C
Nb80-T57C
Y343
Y207
Y217
Y193
Y140
Y231
Y227
Y149*
Y333
114
118
122
15N
9.5
9.0
8.5
8.0
7.5
7.0
[ppm]
1H
B
Nb80-Q39C
Nb80-T57C
experimental PCS
predicted PCS
[ppm]
0
-0.2
-0.4
-0.6
-0.8
-1.0
-1.2
-1.4
-1.2
-1.0
-0.8
-0.6
-0.4
-0.2
0
E
preactive-inactive
active-preactive
CSP [ppm]
0.8
0.7
0.6
0.5
0.4
0.3
0.2
0.1
0
140
149*
193
207
217
227
231
333
343
C
+carvedilol
+isoprenaline
D
+isoprenaline +Nb80
+isoprenaline
F
Y193ECL2
Y207 5.38
Y217 5.48
Y333 7.43
Y227 5.58
Y140 3.51
Y343 7.53
Y231 5.62
Y149ICL2
CSP > 0.25 ppm
CSP < 0.25 ppm

Figure 5

Nanobody GPS by PCS: an efficient new NMR analysis method for G protein coupled receptors and other large proteins

Feng-Jie Wu[1], Pascal S. Rieder[2], Layara Akemi Abiko[1], Philip Rößler[3], Alvar D. Gossert[3], Daniel Häussinger[2], Stephan Grzesiek[1]

[1] Biozentrum, University of Basel, CH-4056 Basel, Switzerland
[2] Department of Chemistry, University of Basel, CH-4056 Basel, Switzerland
[3] Department of Biology, ETH Zürich, 8093 Zürich, Switzerland

Supplementary Material

Supplementary Figures

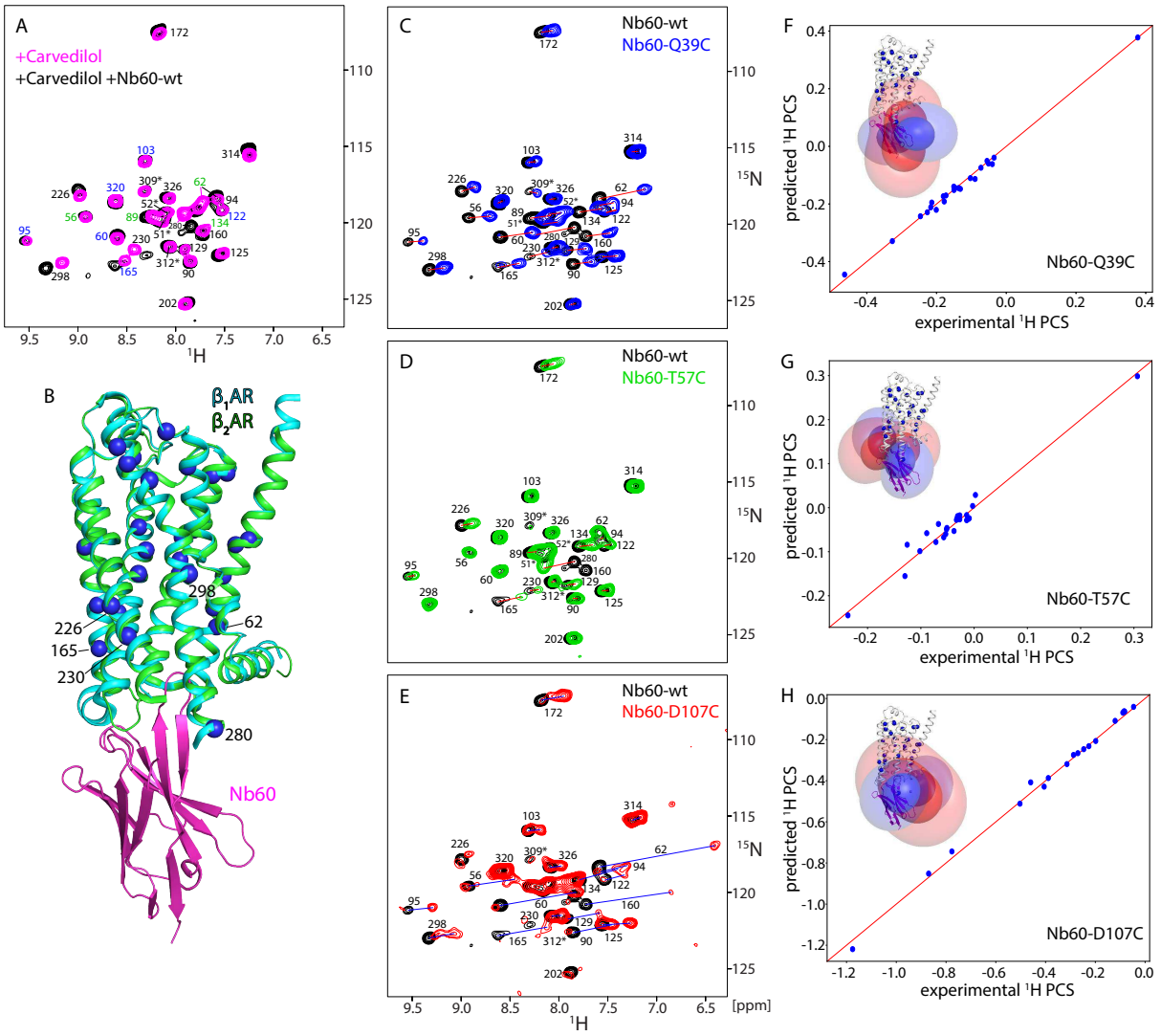

Figure S1. Detection of PCSs induced by three different Nb60-DOTA variants on YY-β_1AR valine residues. (A) ^{1}H-^{15}N TROSY spectrum of ^{15}N-valine YY-β_1AR complexed with carvedilol (magenta) superimposed onto spectrum of ^{15}N-valine YY-β_1AR complexed with both carvedilol and Nb60-wt (black). The labels are color-coded as black for the previously assigned valines through point mutations, green for assignments corrected by GPS-PCS, blue for the assignments newly established by GPS-PCS. (B) Transmembrane helices of the carvedilol·β_1AR complex structure (PDB 4amj, cyan) superimposed onto the helices of the carazolol·β_2AR·Nb60 complex structure (PDB 5jqh, green for β_2AR and magenta for Nb60). Valines are shown as blue spheres. Valines with minor chemical shift changes upon Nb60 binding (see panel A) are marked with residue numbers. (C-E) ^{1}H-^{15}N TROSY spectra of ^{15}N-valine carvedilol·YY-β_1AR in complex with the Nb60-DOTA variants (colored) superimposed onto the spectrum of carvedilol·YY-β_1AR in complex with wild-type Nb60 (black). (F-H) Predicted vs experimental ^{1}H valine YY-β_1AR PCS values for the three different Nb60-DOTA variants according to the final assignments and tensor values. The spatial distributions of the PCS tensors within the β_1AR·Nb60 complex structures are shown on the top left in each figure. Positive (blue) and negative (red) isosurfaces indicate a PCS of 1.0/0.2 ppm (inner sphere/outer sphere).

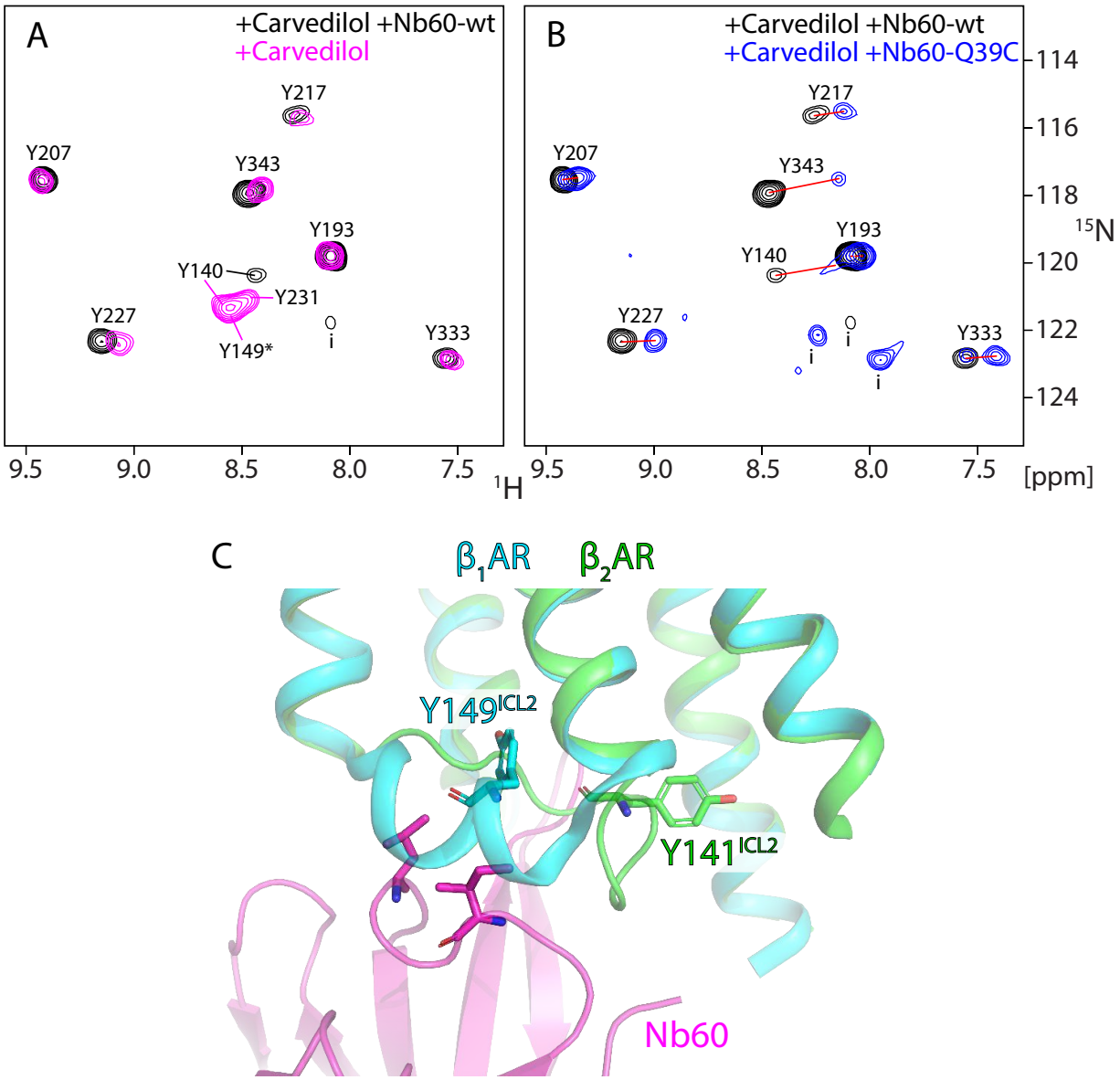

Figure S2. Application of the GPS-PCS method to the assignment of ^{15}N-tyrosines in YY-β_1AR in the inactive state. (A) ^{1}H-^{15}N TROSY spectrum of ^{15}N-tyrosine YY-β_1AR complexed with carvedilol (magenta) superimposed onto the spectrum of ^{15}N-tyrosine YY-β_1AR complexed with both carvedilol and wild-type Nb60 (black). (B) ^{1}H-^{15}N TROSY spectrum of ^{15}N-tyrosine carvedilol·YY-β_1AR in complex with the Tm-DOTA-M7PT-tagged Nb60-Q39C variant (blue) superimposed onto the spectrum of carvedilol·YY-β_1AR in complex with wild-type Nb60 (black). The PCSs are indicated by solid red lines. Resonances marked by 'i' originate from an unidentified low-molecular weight impurity and were insensitive to paramagnetic shifts. (C) Transmembrane helices of the carvedilol·β_1AR complex structure (PDB 4amj, cyan) superimposed onto the helices of the carazolol·β_2AR·Nb60 complex structure (PDB 5jqh, green for β_2AR and magenta for Nb60). The close-up shows the significant reorientation of the tyrosine in ICL2 (Y149^{ICL2} in β_2AR, Y149^{ICL2} in β_1AR) that appears induced by the Nb60 binding.

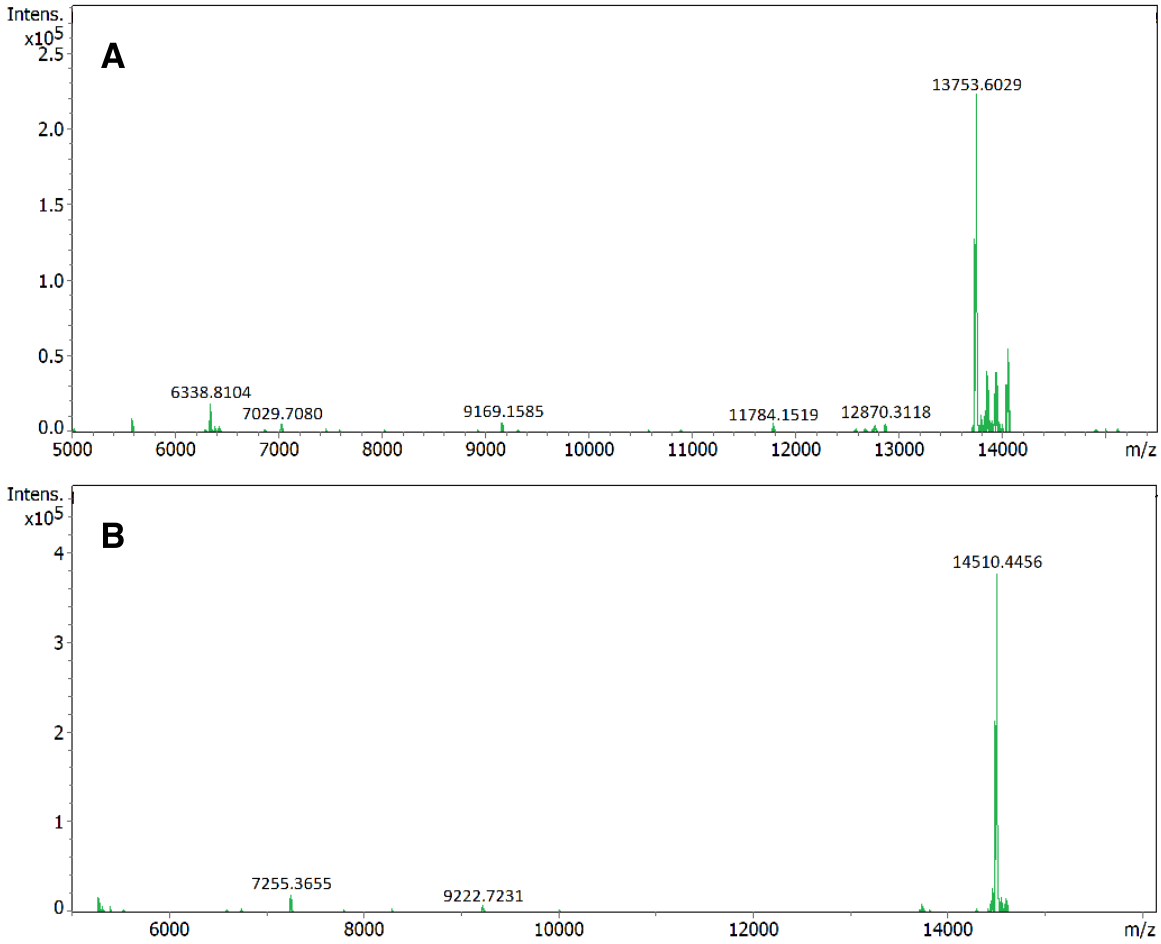

Figure S3: Monitoring of the Tm-DOTA-M7PT labelling reaction of nanobody cysteine mutants by high-resolution time-of-flight mass spectrometry. Example of Nb80-D108C before (**A**) and after (**B**) site-selective spin labelling. **A:** *m/z* for $[Nb80\text{-}D108C+H]^+$ calculated: 13753.6426, detected: 13753.6029; **B:** *m/z* for $[Nb80\text{-}D108C\text{-}Tm\text{-}DOTA\text{-}M7PT+H]^+$ calculated: 14509.8420, detected: 14510.4456.

Supplementary Tables

Table S1: Spin labelling reaction times of the different nanobody single-cysteine mutants determined by high-resolution time-of-flight mass spectrometry. The reaction times vary depending on the accessibility of the cysteine.

nanobody	reaction time [h]
Nb80-S25C	6.0
Nb80-Q39C	7.3
Nb80-T57C	21
Nb80-S70C	6.0
Nb80-N76C	23
Nb80-Y107C	18
Nb80-D108C	12.5
Nb60-Q39C	7.3
Nb60-T57C	64
Nb60-D107C	22

Table S2: Parameters of fitted PCS tensors listed in Paramagpy(Orton et al., 2020) convention: amplitude A_{zz}, rhombicity, metal coordinates (x, y, z), and tensor Euler angles (α, β, γ). The coordinates are given in the coordinate system of PBD 6h7j (Nb80) and 5jqh (Nb60).

	Nb80			**Nb60**		
Tm-DOTA-M7PT variant	Q39C	T57C	D108C	Q39C	T57C	D107C
A_{zz}[1)]	43.305	34.561	62.983	46.534	38.618	56.582
rhombicity[1)]	12.258	12.264	8.465	19.2	16.802	14.101
x[2)]	64.907	53.542	57.832	8.974	26.106	13.268
y	-20.276	-33.787	-23.017	-20.226	-42.201	-20.01
z	-17.98	-44.562	-22.11	-6.344	-18.765	-18.279
α[3)]	108.9	30.369	115.353	137.441	133.186	6.869
β	151.095	53.466	99.92	107.063	68.882	88.426
γ	0.179	40.743	32.919	79.731	177.003	34.756

[1]) in 10^{-32} m^3

[2]) in Å

[3]) in degrees

Supplementary References

Orton, H. W., Huber, T., & Otting, G. (2020). Paramagpy: Software for fitting magnetic susceptibility tensors using paramagnetic effects measured in NMR spectra. *Magnetic Resonance*, *1*(1), 1–12. https://doi.org/10.5194/mr-1-1-2020